Modeling Pyrolysis of Large Coal Particles with Many Species

Jianqing Li
Marquette University

MODELING PYROLYSIS OF LARGE COAL PARTICLES WITH MANY SPECIES

by

Jianqing Li, B.S.M.E

A Thesis submitted to the Faculty of the Graduate School,
Marquette University,
in Partial Fulfillment of the Requirements for
the Degree of Master of Science

Milwaukee, Wisconsin

December 2016

ABSTRACT
MODELING PYROLYSIS OF LARGE COAL PARTICLES
WITH MANY SPECIES

Jianqing Li, B.S.M.E

Marquette University, 2016

Coal currently supplies 40% of the world's electricity needs, and is one of the most important energy sources. As the initial stage of coal combustion, pyrolysis is a thermal decomposition process which converts coal into light gases and tars, which are subsequently consumed in combustion reactions, as well as solid char. Recently there has been interest in using slow pyrolysis as a stand-alone process for the production of chemicals and fuels from large (mm-scale) coal particles.

Simulations can be used to efficiently study the impact of pyrolysis conditions on gas, tar and char yields, as well as gas and tar species compositions, which are an important output for a coal-to-chemicals process. In order to simulate pyrolysis of large coal particles, the Chemical Percolation Devolatilization (CPD) model, which predicts the mass fractions of char, tar and light gas, has been modified and improved. A transient multicomponent vaporization sub-model has been developed to predict the partitioning of heavy species into gaseous tar and liquid metaplast. The Direct Quadrature Method of Moments (DQMoM) is introduced as a computationally efficient method to solve for the evolution of the distribution of tar species as a function of molar mass, and the full discrete tar species distribution can be reconstructed by a novel delumping procedure. Finally, a heat transfer model that can predict temperature gradients within the particles has been incorporated using the finite volume method to discretize the energy equation, with the improved CPD model implemented at every position within the particle.

The results show the necessity of resolving large particles spatially, due to the impact of the local temperature evolution on tar and gas mass fractions and the production of certain species. Higher pyrolysis temperatures result in increased yields of gas and especially large tar species, while decreasing pressures also increase the production of heavier tar species. The agreement between the full discrete species model, which solves differential equations for every tar species, and DQMoM with delumping, which solves many fewer equations, is excellent, while yielding a large improvement in computational efficiency.

.

ACKNOWLEDGEMENT

Jianqing Li, B.S.M.E

Throughout past two and a half years in Graduate School of Mechanical Engineering, I have worked with many talented people, from whom I got a lot of help and direction. First of all, I would like to sincerely thank my advisor, Dr. Simcha Singer, for giving me the opportunity to work on this challenging project. He has given me so much direction and suggestion during the period of research. Moreover, he has encouraged me many times when I felt stuck and upset. As a foreign student, he guided me with patience and encouragement, which made me feel very helpful. Also, I would like to thank my committee, Dr. Casey Allen and Dr. Anthony Bowman, who also gave me many suggestions and helped me a lot on my research.

Next, I would like to thank my colleagues, Rui Gu and Greg Fong, whom I have working with in the thermal lab. Both of them are brilliant colleagues and they have helped me a lot in academic field. Their positive attitude towards working encourages me to work with power. Also they have given me a lot of advice and suggestions for finishing my thesis. Also, I would like to thank my friend, Yi Cai, who is working on his graduate study in University of Pennsylvania. His advice about my course study in past two years gave me a lot of help.

Last, but not least, I would like to thank my parents, who give me the funding and support me to finish my graduate study. Their suggestions and encouragement about the study and life are very important and useful for me. They are the best parents in the world. Finally, I would like to thank my girlfriend, Yuxing Zhang, for her love, understanding and support during my amazing graduate-student life.

TABLE OF CONTENT

LIST OF TABLES

LIST OF FIGURES

Chapter I. Introduction

As one of the most important energy sources, coal currently supplies 40% of the world's electricity needs, making it the primary source for electricity generation (IEA 2015). Typical air combustion of coal is the most common method used in power plants for generating thermal energy and subsequently electric energy, which is used in most aspects of our lives. Generally, coal combustion can be divided into two stages: devolatilization and char combustion.

Devolatilization, or pyrolysis, is the initial stage of coal combustion, and is the thermal decomposition (without any reaction with oxygen) of coal into volatiles (consisting of light gases and heavier tars) their escape from the particle and in some cases, their subsequent reaction.[5] Pyrolysis can also be used as a stand-alone process, with interest in employing large (millimeter scale) coal particles to produce chemicals that could subsequently be used for fuels. If pyrolysis chemicals are to be used for making fuels, it is important for a pyrolysis model to predict the detailed species composition of the product gases. Also, temperature gradients should be considered for such a process, based on the relatively large size of the particles.

The Chemical Percolation Devolatilization (CPD) model has been used in several studies to model coal devolatilization (see Chapter II).[5] It describes the pyrolysis behavior of coal based on the chemical structure of the parent coal and can predict the fraction of tar, which is a mixture of large vapor species, and of light gas, which are generated during the process of pyrolysis. The general CPD model describes the process of pyrolysis by

ignoring any temperature gradients within the particle, since they are typically negligible for the small particles employed in coal fired power plants.

With the goal of modeling stand-alone pyrolysis of large coal particles for chemicals production, this thesis presents three improvements to the CPD model.

1. Internal temperature gradients may play a significant role in the pyrolysis of large-scale particles. Being a series of thermochemical decomposition reactions, the rate and products of pyrolysis can be influenced significantly by the *local* temperature.[13] Every different position inside of a large particle has a unique temperature. So the temperature gradient plays an important role in pyrolysis of large scale particle. Thus, compared with the general CPD model used for small scale particle, the generation of tar and gas should be considered at different positions inside of the large particle due to the temperature gradient. Thus, if we research the pyrolysis of large particles with a spatially varying temperature, the accuracy of CPD model can be improved and used on different sizes of coal particles. Therefore, based on this motivation, a one improvement to the CPD model developed in this thesis is a description of the process of pyrolysis in a large coal particle. Based on the heat transfer theory, the conservation equation of thermal energy is used in the model to make the temperature a function of position within the particle, instead of a single temperature for all points.

2. A multicomponent vapor-liquid equilibrium (VLE) sub-model is included in the existing version of the CPD model. It represents the partition of the molecular fragments generated by thermal decomposition into liquid (“metaplast”) species, which remain in the particle and eventually solidify, and vapor species, which escape as tar. VLE is a special condition that a liquid and its vapor are in phase equilibrium with each other, at the given

temperature and pressure.[5] However, the previous VLE sub-model incorporated in the CPD model has the disadvantage that it is not very easy to combine into a simulation based on ordinary differential equations. More importantly, as the developers of the CPD model noted, in the original model, *V/F*, which is the fraction of total vapor produced, is time-step dependent, meaning that as the numerical time step increases, *V/F* increases.[22] Therefore, an improved VLE model is applied in this thesis to eliminate the time-step dependence and improve the accuracy of the model, especially for many discrete species. This modified method is based on a transient vaporization process and predicts *V/F* and the generation of discrete tar species, and is more accurate than the previous (time-step dependent) method.

3. Finally, the original CPD model only predicts the mole fractions of different tar species in terms of fragment size separated into very wide molecular weight bins. However, it has been proven by the experiment that there are many discrete species generated during the process of pyrolysis.[13] While the knowledge of detailed species is important for pyrolysis for chemicals production, the original CPD model cannot predict the distribution of discrete tar species as a function of time and temperature.

Using the modified VLE model that will be described in Chapter III, it is possible to incorporate the generation of arbitrarily many discrete tar species into the CPD model. However, it costs too much computational time to solve more than 500 ordinary differential equations (ODEs) for each discrete species. Therefore, it is necessary to find an alternative way to solve these complicated ODEs. The Quadrature Method of Moments (QMoM) is a general method used to evolve distributions, such as the many tar species generated by pyrolysis.[11,12] The Direct Quadrature Method of Moment (DQMoM) is also an effective method developed from QMoM and is employed in this thesis to solve for the distribution

of tar species in a computationally efficient manner.[2,26] Most importantly, after solving the DQMoM model, a novel delumping procedure is applied to recover the data on individual, discrete species from the distribution of species solved by DQMoM. In summary, the goal of combining the DQMoM and a delumping step is saving the computational time for predicting the detailed tar species compared with the CPD model.

This thesis introduces the three main improvements to the CPD model described above and presents result from the improved CPD model. The model is built and simulated based on MATLAB and the extension tool named "Sundials IDA Solver", which can solve the Ordinary Differential Equations (ODEs) and the Differential Algebraic Equations (DAEs).

Chapter II contains a literature review for the necessary background. First, general information about pyrolysis will be summarized. Also, the general CPD model is reviewed to prepare for the following development. The finite volume method and VLE method will be reviewed as the background to use in the improved CPD model. Finally, QMoM and DQMoM are also introduced as an important part of the background.

Chapters III presents the improved CPD model. This new model is developed based on the original CPD model and incorporates three improvements. The temperature profile inside of the particle will be modeled based on the conservation equation, and solved by the finite volume method. Then the process of modeling improved CPD model with new VLE method will be fully explained. This new VLE method eliminates the time-step dependence and describes the process of pyrolysis as a transient and continuous condition.

Chapter IV introduces the computationally efficient method to solve for discrete tar species generated by pyrolysis, using DQMoM with delumping. The DQMoM method will

be applied to solve differential equations for the distribution of tar species based on weights and nodes of different “lumped” species and the delumping method will then extract the discrete species from the result of “lumped” species.

The results of improved CPD model with VLE method and DQMoM model with delumping method are presented and discussed in Chapter V. The results for the change of chemical properties, including different kinds of bridges which are broken and generated during the process of pyrolysis will be provided. Also the temperature profile solved by finite volume method is shown in this chapter. Results for discrete species generated by the DQMoM + delumping model will be presented and discussed. What is more, a comparison between DQMoM + delumping and the full discrete species model (exact compared to DQMoM + delumping) will be made.

The last part of this thesis is the conclusion and suggestions for future work. These include the advantages of the improved CPD model and the ideas to improve model efficiency and accuracy in the future.

Chapter II. Literature Review

This chapter is a review of previous studies related to our improved CPD model. The goal of the literature review is to present the basics of the CPD model, the finite volume method, the vapor-liquid equilibrium sub-model and the DQMoM approach.

A. Chemical Percolation Devolatilization (CPD) Model

Pyrolysis is the thermal decomposition process which partitions coal (or other solid fuels) into volatiles (light gases and tars) and solid char in the absence of oxygen. During pyrolysis, liquid phase fragment molecules are produced by decomposition reactions. Some of them vaporize and leave the particle as tar, meanwhile others remain as liquids and eventually solidify to form char. Thus, in terms of individual gaseous species, the composition and rate of evolution are significant, which will influence the composition of products during coal pyrolysis.[10] Moreover, to research the details of pyrolysis of large coal particles, the process of heat transfer inside of the particle must be considered.[24]

There have several different pyrolysis models which have been published. A mathematical model which describes the pyrolysis behavior of small scale coal particle has been formulated. It uses a constant pyrolysis rate and predicts the behavior of different types of coal which have been compared with experiment.[3] Another pyrolysis model, which uses a single kinetic rate to describe pyrolysis is introduced , using a single Arrhenius type rate expression.[6] With the analysis of chemical structure of coal being used in the field, models based on the coal's chemical structure were developed and included a flash distillation model to describe the partitioning of fragments into tar and liquid using a vapor-liquid equilibrium process.[8] This model is called FLASHCHAIN.

The Chemical Percolation Devolatilization model, which is known as the CPD model, has proven an accurate and effective model to describe the pyrolysis behavior of coal based on the initial chemical structure of the coal.[1 5 10 14] Percolation theory is a method in statistical physics and mathematics which can describes the behavior and connectedness of clusters in a random graph.

The complex macromolecular structure of coal consists, broadly, of clusters of fused aromatic rings connected by bridges and containing dangling side chains, as illustrated in Fig. 2-1.[5] The thermal decomposition that occurs during pyrolysis breaks these bridges and produces molecular fragments of various sizes, which is analyzed and simulated using percolation theory. A fragment is a group of species which are generated from bridge breaking of cluster and have similar finite molecular weight. Therefore, it is very important, in using the CPD model, to know the initial structure of the coal macromolecule (in a statistical sense).

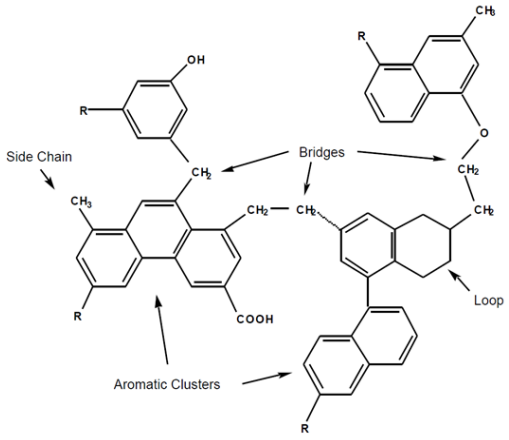

Figure 2-1. Representative chemical structures identified in 13C NMR analyses and used in the description of coal and coal chars in the CPD model [6].

The CPD model therefore requires coal-dependent input parameters taken from chemical characteristics of the parent coal, wherever possible. Four of the five coal-dependent chemical structure parameters in the CPD model can be taken directly from NMR analyses of the parent coal, if available. These parameters will be used in calculating the parameters of the coal based on the structure, such as the number of initial labile bridges, the average mass of a fused ring site and the mass of bridges.[5]

Bethe lattice statistics are implemented with analytical mathematical functions to describe the evolving structure of the coal during pyrolysis. Bethe lattices are a class of lattices which are characterized by a coordination number and a bridge population parameter connected only by a single path of bridges and sites.[5] In other words, Bethe lattices have no loops. In coal pyrolysis, Bethe lattices have an analytical solution for the statistics of bridge dissociations and are a tractable method to analyze different cluster sizes for molar distribution of tar and light gases fragments.[5]

Using Bethe lattice statistics, the initial coal characterization and a reaction scheme to describe the breaking of bridges during pyrolysis, the distribution of fragments as a function of size and the fraction of material in the infinite char array are expressed through percolation theory. A distinction between low molecular weight aromatic fragments that vaporize as tar and high molecular weight fragments that remain with the char in a liquid or solid state as metaplast is made using a vapor-liquid equilibrium submodel.[5] Parameters based on the chemical structure of a particular lignite (low rank coal) particle are shown in Table 2-1. All of these parameters will be used in the improved CPD model.

Recently, a more detailed version of the CPD model has been developed for the release of light gas. This model provides expressions for formation of particular light gas

species and includes differential equations for each to augment the CPD model.[17] These equations for light gas species are included in the model developed in this thesis.

Table 2-1. Parameters used in CPD model

Notation	Definition	Value	Unit
P_0	The fraction of attachments that are bridges	0.61	
C_0	Char bridges	0	
$\sigma+1$	The average number of attachments (i.e., side chains and bridges) per cluster	4.6	
M_{del}	The average molecular weight per side chain	22	*g/mol*
MW_{cl}	The average molecular weight per aromatic cluster	267	*g/mol*

B. Vapor-Liquid Equilibrium Model

As mentioned above, to predict the fraction of each fragment size that enters the vapor phase (as tar), or which remains in the coal particle as liquid (metaplast) and eventually solidifies as char, a vapor-liquid equilibrium sub-model has been incorporated in the CPD model.[22] The basic idea of this sub-model is to treat the fragments generated by bridge breaking as the feed stream in a flash equilibrium process, while using Raoult's law to relate liquid and vapor mole fractions. Raoult's Law is a thermodynamic expression which describes the effect of vapor pressures on gas phase pyrolysis products. Also, assuming the mixture is an ideal mixture, the partial pressure P_i of a substance is equal to the product of the vapor pressure of the pure substance P_i^v and the mole fraction of the substance in the liquid x_i:

$$P_i = y_i \cdot P = x_i \cdot P_i^v \tag{2.1}$$

where y_i is the mole fraction of the species in the vapor phase.

Next, the approach to flash distillation has been developed by King to model vapor-liquid equilibrium.[31] During the flash process, the feed divides into two separate phases. Some fragments vaporize and leave the vessel (particle) as vapor phase tar, others remain in the vessel in the liquid phase. Fig. 2-2 shows that the basic idea of the vapor-liquid equilibrium in a "flash vessel" in the original CPD model.[22]

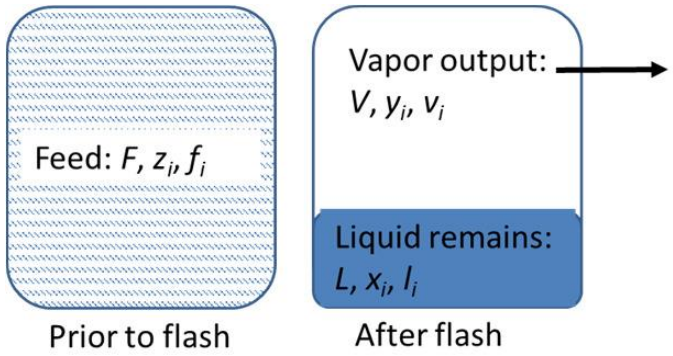

Figure 2-2. "Flash Vessel" used for vapor-liquid equilibrium in the CPD model

Prior to flash, the feed is a mixture with different fragments, and F is the total moles of fragments per cluster before vapor-liquid equilibrium. What is more, f_i represents the moles of fragment i per cluster before vapor-liquid equilibrium, and z_i is the mole fraction of each fragment of size i per cluster in the flash vessel prior to flash. Therefore, it has a simple relationship that:

$$f_i = z_i \cdot F \tag{2.2}$$

After the flash process, V is the total moles of fragments in vapor phase, v_i is the moles of fragment i in vapor phase, and y_i is the mole fraction of each fragment in the vapor phase. So, like Eq. 2.2, the relationship is:

$$v_i = y_i \cdot V \tag{2.3}$$

Similarly, L, l_i, x_i represent the total mole of fragment of liquid, moles of liquid fragment i, and the mole fraction of each fragment in the liquid phase after vapor liquid equilibrium. The equation for the liquid phase is:

$$l_i = x_i \cdot L \tag{2.4}$$

And F, V, and L are the sum of the f_i, v_i, and l_i. For mass conservation, before and after the flash process, the total moles of fragment are same. So,

$$F = V + L \tag{2.5}$$

The relationship in Eq. (2.1) between the mole fraction of species in vapor phase y_i and in liquid phase x_i, can be expressed as [5]

$$y_i = K_i \cdot x_i \tag{2.6}$$

where the phase equilibrium constant, K_i, accounts for the vapor pressure of a given species, and for the numerous species in coal tar, is based on a correlation developed by Unger and Suuberg[5] as a function of temperature and molecular weight and is given in Chapter 3.

C. Energy Equation and the Finite Volume Method

The CPD model is a local kinetic model which can describe the process of the pyrolysis of coal particle in the absence of any heat transfer limitations. This is acceptable if the particle size is small enough (for example, less than 100 micrometers for pulverized coal combustion conditions), and/or the gradient of temperature can be neglected or is irrelevant. On the other hand, if the particle is larger, the temperature inside of the particle

varies with the position within the particle, and this effect has to be considered in order to obtain an accurate result for the pyrolysis process. Thus, the energy conservation equation can be applied with the CPD model to solve for the temperature distribution in large particle. The general form of conservation equation of energy is:

$$\left(\rho c_p\right)_{eff}\frac{\partial T}{\partial t}+\rho c_p \boldsymbol{u}\cdot\nabla T=\nabla\cdot\left(k_{eff}\nabla T\right)-\Delta h Q_{solid-to-gas} \tag{2.7}$$

The energy equation is a partial differential equation, which has several terms, including a convection term and a diffusion term and is difficult to solve analytically. Therefore, an appropriate numerical method to solve the differential equation is important to get an accurate temperature distribution inside of the particle. The finite volume method is a good method to solve differential equations. It is a method for representing and evaluating differential equations in the form of algebraic equations. The finite volume method can discretize a governing differential equation, yielding an algebraic relation connecting the value of dependent variable φ for a group of grid points.[18,25]

For one dimensional problem, Fig. 2-3 shows the basic idea of the finite volume method.[25] The grid point P has two neighboring grid points, E and W. The control volume is located between the two dash lines.

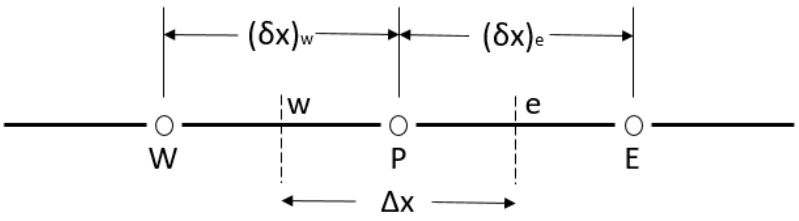

Figure 2-3. Grid-point cluster for the one-dimensional problem

For example, assume the governing equation is the steady one dimensional heat conduction equation:

$$\frac{d}{dx}\left(k\frac{dT}{dx}\right)+S=0 \tag{2.8}$$

This is a second order differential equation. First, for a one dimensional problem, the volume of control volume depends on the distance Δx. So, integrate the Eq. 2.8 and rearrange the equation:

$$\left(k\frac{dT}{dx}\right)_e-\left(k\frac{dT}{dx}\right)_w+\int_w^e S dx=0 \tag{2.9}$$

k_e and k_w are the thermal conductivity coefficients at the point *e* and *w*. Then use the approximation method of derivative to express the derivative terms in Eq. 2.9. To express the variation of the dependent variable between the grid points, the piece-wise linear profiles are used to evaluate the derivatives:[7]

$$\frac{k_e(T_e-T_p)}{(\delta x)_e}-\frac{k_w(T_p-T_w)}{(\delta x)_w}+\bar{S}\Delta x=0 \tag{2.10}$$

Now Eq. 2.10 is the discretized equation which comes from the differential Eq. 2.8 for the control volume method. And $\bar{S}$ is the average value of *S* over the control volume.[25]

Therefore, if the energy equation is required to solve the temperature distribution inside a large-scale particle, it is easier to use the finite volume method to convert the difficult differential equation to the discretization equation than solving the differential equation directly for arbitrary boundary conditions, initial conditions and potentially nonlinear source terms associated with the heat of pyrolysis. After we know the boundary

conditions for the discretization equation, the numerical method can solve the equation and get an approximation solution.

D. Direct Quadrature Method of Moments

During the process of pyrolysis, many different species are generated as the process progresses. In the CPD model, the mole fraction of tar species is calculated by separating them into different fragment sizes, using very coarse bins. However, if we want to find the actual species distribution within those fragment bins (more than 500 species have been generated during a detailed kinetic pyrolysis simulation at MIT using Monte Carlo simulation) that escape the particle as tar, the VLE calculation can become very computationally expensive. Therefore, an alternative way to solve the problem is to represent the numerous tar species as a *distribution* of molecular weight using a method of moments instead of solving ODEs for each species directly.[12] Subsequently, a reconstruction procedure will be developed to obtain the evolution of each species in a computationally efficient manner.

The continuous thermodynamics theory, which has been developed by Laurent and Cotterman, can be used for analyzing pyrolysis.[4,13] This theory uses a continuous distribution function to describe the chemical composition of a mixture which contains an infinite number of components. Furthermore, the equilibrium properties, which are some characterizing properties, are described upon extension of well-known thermodynamic methods.

The Quadrature Method of Moment (QMoM) is a general way to solve for the evolution of a distribution by tracking several of its moments.[11] It derives from the conventional moment problem and the moment evolution equations.[15] It can be applied for

different modeling, such as aerosol dynamics,[16] population balance equations,[26] and multi-component spray vaporization.[12] The basic QMoM theory will be presented for a distribution which evolves according to an ordinary differential equation:[26]

$$\frac{\partial n(\xi;t)}{\partial t} = S(\xi;t) \tag{2.11}$$

The left hand side function $n(\xi;t)$ is the Number Density Function (NDF), which can represent the expected number of particles per unit volume. In terms of mole fraction, we can get the similar expression $x(\xi;t)$, where the internal variable ξ represents the molecular weights produced by pyrolysis and *t* represents the time. Therefore, the Eq. 2.11 can be updated based on mole fraction:[26]

$$\frac{dx(\xi;t)}{dt} = S(\xi;t) \tag{2.12a}$$

QMoM applies a moment transform to Eq. (2.12a), which yields

$$\frac{dm_k(\xi;t)}{dt} = \overline{S_k}(\xi;t) \tag{2.12b}$$

The right hand side is the source term which is a function of mole fraction. It can be solved by a Gaussian quadrature formula:[26]

$$\overline{S_k} = \int_0^{+\infty} S(\xi)\xi^k d\xi = \int_0^{+\infty} x(\xi)f(\xi)d\xi \approx \sum_{\alpha=1}^{n} w_\alpha f(\xi_\alpha) \tag{2.13}$$

where w_α and ξ_α are respectively the weights (mole fraction) and nodes (molecular weights) and *n* is the number of nodes used for the interpolation. The advantage of QMoM

is that any arbitrarily shaped distribution may be employed and the accuracy of the quadrature approximation can be improved with only a few nodes.[15,26] Also, it can be implemented relatively easily numerically.

Recently, based on the theory of QMoM, another method has been developed, which is named Direct Quadrature Method of Moment (DQMoM). It has been used in a few different fields, include aerosol particles[9] and multicomponent droplet spray vaporization.[2] The basic idea of DQMoM is similar to the QMoM. Based on the last equality in Eq. (2.12b), the mole fraction in QMoM is equivalent to a summation of *n* Dirac delta functions:[26]

$$x(\xi;t) = \sum_{\alpha=1}^{n} w_\alpha(t)\delta[\xi - \xi_\alpha(t)] \tag{2.14}$$

Combine Eqs. 2.12 and 2.14, the partial differential equation based on DQMoM can be derived:

$$\sum_{\alpha=1}^{n} \frac{\partial}{\partial t}[w_\alpha \delta(\xi - \xi_\alpha)] = \overline{S_k} \tag{2.15}$$

The right hand side source term function is the same as in Eq. 2.13 and it also can be solved by quadrature approximation. For the left hand side, it can be expended by using derivative rules and calculations:[26]

$$\sum_{\alpha=1}^{n} \delta(\xi - \xi_\alpha)\left[\frac{dw_\alpha}{dt}\right] - \sum_{\alpha=1}^{n} \delta'(\xi - \xi_\alpha)\left[\frac{d(w_\alpha\xi_\alpha)}{dt} - \xi_\alpha\frac{dw_\alpha}{dt}\right] = \overline{S_k} \tag{2.16}$$

Define two notations for convenience:

$$\frac{dw_\alpha}{dt} = a_\alpha; \quad \frac{d(w_\alpha \xi_\alpha)}{dt} = b_\alpha \tag{2.17}$$

Then the Eq. 2.16 can be simplified to a linear system of ODEs with the moment transfer and the simple rule for Dirac functions. The result is as follow:

$$(1-k)\sum_{\alpha=1}^{n} \xi_\alpha^k \, a_\alpha + k\sum_{\alpha=1}^{n} \xi_\alpha^{k-1} \, b_\alpha = \int_0^{+\infty} S(\xi)\xi^k d\xi = \overline{S_k} \tag{2.18}$$

From Eq. 2.18, for the value of *k*=1, 2, 3…, this system can be expanded to matrix form and solved, where the source term vector is from using the quadrature.

In total, comparing QMoM and DQMoM, they are mathematically equivalent. But DQMoM has the advantage that it can get the solution without resorting to the Product-difference algorithm, which may become unstable.[14] Moreover, because DQMoM can use the matrix to describe the system of original differential equations, it can solve them more efficient and inexpensive computationally. More important, DQMoM model has been demonstrated to use for continuous thermodynamics problem, and the solution from DQMoM model is more accurate and stable than QMoM.[9] Therefore, DQMoM will be used for coal pyrolysis simulation to get the distributions of tar species generated.

Chapter III. The Improved CPD model

This chapter introduced the improved CPD model for large coal particles. The improved model is developed based on the general CPD model and vapor-liquid equilibrium theory to describe pyrolysis with transient vaporization of tar. The mole fraction of every generated species during pyrolysis can be simulated. What is more, the finite volume method is also used to solve the energy conservation equation and get the continuous temperature profile, which is used locally in the CPD model.

A. Model Description

This model is developed based on a large (mm-scale) lignite particle, which means that temperature gradients may influence the process of pyrolysis for typical heating rates. Due to the complicated situation in real coal pyrolysis, the particle can be simplified as a one-dimensional, spherically symmetric particle. Next, the modeled particle is viewed as porous, similar to the real situation. Also, this model can be applied in different types of large coal particles, and the necessary input parameters was introduced in Chapter II.

B. CPD Model

In this section, the reaction terms in the basic CPD model are presented. The general CPD model can describe the initial thermal decomposition of coal into different volatiles, including light gases and heavier fragments, and account for partitioning of the fragments into vapor (tar) and liquid (which eventually forms char).[5] As mentioned above and as shown in Fig. 2-1, it is clear that there are different kinds of bridges in the structure of coal. Different aromatic clusters are interconnected by the bridges. Bridges can be divided into labile and charred bridges. Labile bridges are unstable and break during coal pyrolysis. On

the other hand, char bridges are more stable because they can remain intact at a higher temperature. So, the characteristics of bridges shows that the temperature can influence coal pyrolysis.[5] The chemical reaction scheme in the CPD model is shown in Fig. 3-1 and discussed next.[10]

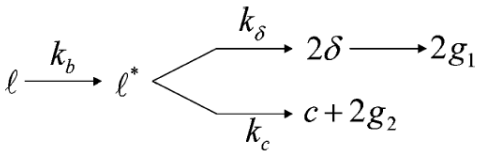

Figure 3-1. Chemical Reaction Scheme in the CPD model

A labile bridge can break in two different ways to generate two kinds of light gas after the stable bridge decomposes to a reactive bridge intermediate, l^*, which is unstable and reacts quickly. In one reaction pathway, it is stabilized to form a char bridge, and the kinetic expressions for the evolution of the number of labile bridges and char bridges are:

$$\frac{dl}{dt} = -k_b \cdot l \tag{3.1}$$

$$\frac{dc}{dt} = \frac{k_b \cdot l}{\rho + 1} \tag{3.2}$$

where *l* and *c* represent the labile and char bridge, k_b is the reaction rate of bridge breaking, and ρ is composition rate coefficient. Both of them have the units of 1/s.[5]

Next, another reaction pathway indicates that the bridge is stabilized to produce side chains from the reactive bridge fragment. Then the side chains can be divided into precursors for a variety of light gases.[5] The kinetic expression for the evolution of the number of side chain is:

$$\frac{d\delta}{dt} = \frac{2 \cdot \rho \cdot k_b \cdot l}{\rho + 1} - k_g \cdot \delta \tag{3.3}$$

where δ is the side chain, with k_g is the reaction rate for the gas release steps, which the unit is also 1/s.

Furthermore, in Eq. 3.1 to 3.3, k_b is the reaction rate of bridge breaking, which can be expressed as:[5]

$$k_b = A_b \cdot exp\left(\frac{-E_{min,b}}{\bar{R} \cdot T}\right) \tag{3.4}$$

$$E_{min,b} = E_b + \sigma_b \cdot N\left(1 - \frac{l}{l_0}\right) \tag{3.5}$$

where A_b is the bridge scission frequency factor, $E_b$is the bridge scission activation energy which is normally distributed, and σ_b is standard deviation for distributed E_b. Accordingly, the notation *N* in Eq. 3.5 represents the normal inverse function. It is very useful function in statistics field. Parameter L_0 is the initial value of labile bridges. Based on the feature of distribution E_b, the use of the normal inverse function can get more accurate results of k_b with the time change.

Due to the labile bridge breaking, some bridge material is stabilized to produce side chains δ from the reactive bridge fragments. These can be further divided into precursors for a variety of light gases. Based on the Appendix, 17 light gas species are applied in the CPD model. The expression of the reaction rate for the gas release, k_g for each precursors is as follows:[5]

$$k_{g,i} = A_i \cdot exp\left(\frac{-E_{min,i}}{\bar{R} \cdot T}\right) \tag{3.6}$$

$$E_{min,i} = E_i + E_{\sigma,i} \cdot N\left(\frac{g_i}{2 \cdot f_{g_i}/f_{g_{tot}} \cdot (1 - c_0)}\right) \tag{3.7}$$

For these two equation, E_i is the effective activation energy and $E_{\sigma,i}$ is the standard deviation for each precursor. And A_i is the frequency factor for each precursors. What is more, f_{g_i} is the functional gas species source fraction, which is different for every single precursors and the value can be found in Appendix. Another internal variables, g_i represents the amounts of various light gas species and it is a function of labile bridge *L*, initial charred bridge c_0, and the side chains δ_i. And the mass fraction of light gas is shown in Eq. 3.9

$$g_i = 2 \cdot (1 - L - c_0) \cdot \frac{f_{g_i}}{f_{g_{tot}}} - \delta_i \tag{3.8}$$

$$f_{gas} = \frac{r_{ba} \cdot g_{total} \cdot (\sigma + 1)}{4 + 2 \cdot r_{ba} \cdot (1 - c_0)(\sigma + 1)} \cdot (1 - f_{tar}) \tag{3.9}$$

In Eq. 3.9, f_{tar} is the mass fraction of tar generation which will be solved by differential equation later, r_{ba} is ratio of mass of bridges to mass of aromatic materials,[5] and $\sigma + 1$ is the average number of attachments mentioned in Table 2-1. On the other hand, in the general CPD model, the species which has similar molecular weights are seen as big "fragments" and this can be regarded as the "mock" x_i instead of the discrete species. Each fragment has different sizes due to the different structure of the fragments. It can contain one aromatic cluster, which means size *n*=1, or size *n=2* fragments represents two clusters connected by a labile or char bridge, or *n* clusters connected by *n-1* bridges. And the mass of these finite fragment of size *n* can be calculated based on the general CPD model: [5]

$$m_{frag,n} = n \cdot m_a + (n-1) \cdot m_b \left(\frac{l}{p}\right) + \frac{\tau \cdot m_b \cdot \delta_{tot}}{4(1-p)} \quad (3.10)$$

These fragment are generated by the labile bridge breaking so that it depends on the bridge population parameters, labile bridge *l* and the fraction of intact bridge *p,* which is the summation of the labile bridge and charred bridge. Furthermore, the total mass of each cluster is determined by the structure of the cluster:[5]

$$m_{total} = m_a + m_b \cdot (1 - c_0)(\sigma + 1)/2 \quad (3.11)$$

where m_a is the average mass of the fused ring site and m_b is the mass of bridges. Parameter τ in Eq. 3.10 is the number of broken bridges on the perimeter of an *s*-bridge cluster. They are given by:[5]

$$s = n - 1 \qquad \tau = n(\sigma - 1) + 2 \quad (3.12)$$

The last part of this section introduces the ordinary differential equations for the cross-linked metaplast and the total tar mass fraction. During pyrolysis, much of the original coal particle decomposes and is released as volatile matter. The liquid (metaplast) that remains in the particle (from the VLE sub-model) is cross-linked to the char matrix before pyrolysis ends.[5] Based on the mass of fragments, the average molecular weights of tar, tar and light gas, and metaplast, are as follows:

$$MW_{avg,tar} = \frac{m_{frag,n} \cdot y_n}{1 - y_{gas}} \quad (3.13)$$

$$MW_{avg,tar,gas} = y_{gas} \cdot MW_{gas} + m_{frag,n} \cdot y_n \quad (3.14)$$

$$MW_{avg,meta} = x_{gas} \cdot MW_{gas} + m_{frag,n} \cdot x_n \quad (3.15)$$

So, the ODEs for mass fractions of tar and cross-linked metaplast can be derived:

$$\frac{df_{tar}}{dt} = \frac{d\left(\frac{m_{tar}}{m_{total}}\right)}{dt} = \left(1 - y_{gas}\right) \cdot \frac{\dot{V} \cdot MW_{avg,tar}}{m_{total}} \tag{3.16}$$

$$\frac{df_{cross}}{dt} = -\frac{d\left(\frac{m_{meta}}{m_{total}}\right)}{dt} = k_{cross}\frac{m_{meta}}{m_{total}} = k_{cross}\frac{L^{*} \cdot MW_{avg,meta}}{m_{total}} \tag{3.17}$$

where the unknown variables, x_n and y_n, represent the between the mole fraction of fragment in vapor phase and in liquid phase, respectively. Similarly, x_{gas} and y_{gas} represent the mole fraction of light gas in the liquid phase and in the vapor phase. The average molecular weight of light gas, MW_{gas}, is equal to half the bridge mass $m_b/2$.[5] All of these variables can be calculated together with the improved VLE model which will be introduced in section E.

C. Discrete Species Distribution in the CPD Model

At this point, all the discussion about tar in the original CPD model has been about fragments, rather than discrete species. The final amounts of *discrete* feed species, f_i (see Eq. 2.2), generated by bridge-breaking has been obtained by the MIT model mentioned above for a single coal under a single condition. Somehow, if one could obtain the discrete species generated for any coal at any time, it could be used in the improved VLE sub-model described in Section E to get the mole fraction of discrete tar species, y_i, at every time step.

The method that will be outlined in this section to determine the discrete f_i at all times can be thought of as a framework to demonstrate the improved VLE to be described in Section E. In the future, an improved method based on more detailed kinetics of bridge-breaking and coal structure characterization could be developed to determine all discrete f_i.

Based on the definition of a fragment, each fragment contains various amounts of species with similar molecular weight (a bin) and the number fraction of each fragment changes during pyrolysis. Also we know the number fraction of the discrete species at the final time for the particular coal studies at MIT. Therefore, if we connect the number fraction of fragments with the number fraction of discrete species at the final time, we can estimate approximately the number fraction of discrete species generate at every single time. The relationship of all the number fraction of discrete tar species between each time step to the final time step is:

$$w_j(t) = z_{i,f} \cdot \frac{w_j(t_{final})}{\sum w_{j,i}} \tag{3.18}$$

where $w_j(t_{final})$ is the number fraction vector of the discrete species at the final time, $\sum w_{j,i}$ is the sum of the w_j in terms of the size of fragment i at every time step, and $z_{i,f}$ is the number fraction of each fragment of tar. However, with the time goes by, the size of fragments may change according to the CPD model and the range may change at the same time. In this work, it is solved by connecting $\sum w_{j,i}$ with $m_{frag,n}$. Specifically, the result of $\sum w_{j,i}$ with respect to z_i is determined by the average of every two neighbor fragments at every time step. For example, if the value of m_{frag} of size 1, 2, and 3 at specific time are 300, 600, and 900 *g/mol*, then the result of $\sum w_{j,i}$ with respect to z_2 is the sum of w for all the discrete species with molecular weight between 450 and 750. Because $m_{frag,n}$ is time dependent, $w_j(t)$ is also time dependent variable. Therefore, the detailed vector for w_j at every time step can be derived and will play an important role in the improved VLE model. The final amounts of *discrete* feed species is then $f_j = w_j F$.

D. Particle Temperature

For pulverized coal combustion and gasification, the influence of temperature can be ignored in the general CPD model because the particle size is small enough such that spatial variations are negligible. However, a larger particle is considered in this pyrolysis-only application, and the temperature is different at every position inside of the particle. Therefore, temperature gradients inside of the particle should be modeled to describe the influence of local temperature on the process of pyrolysis.

In this improved model, the thermal energy conservation equation is used to determine the temperature profile. The thermal energy equation, which is based on Eq. 2.7 is:

$$\left(\rho c_p\right)_{eff}\frac{\partial T}{\partial t} = \nabla\cdot\left(k_{eff}\nabla T\right) - \rho c_p \boldsymbol{u}\cdot\nabla T + H\frac{\partial \rho}{\partial t} \tag{3.19}$$

where ρ_{eff} is the density of coal particle and c_p is the specific heat capacity of coal particle. In the porous coal particle, c_p is a weighted average of the specific heat capacity of coal and air. The first term of right hand side is the heat conduction term, and k_{eff} is the effective thermal conductivity of the coal particle. The second term on the right hand side is the convection term, where $\boldsymbol{u}$ is the velocity of the gas, which has unit of *m/s*. The last term on the right hand side is the heat of reaction generated from the pyrolysis, where H is the heat of pyrolysis.

Because the temperature inside of the particle is a function of distance, r, in one dimension from the selected point to the particle center, the finite volume method is applied to discretize the heat conduction and convection term. Obviously, the heat conduction term

is a second order term. Fig. 3-2 shows the finite volume method used for the discretization of the conduction term.

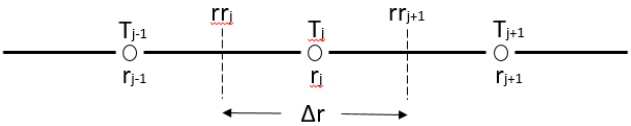

Figure 3-2. Finite volume method in conduction term

T_j is the temperature of the specific point, j, T_{j-1} and T_{j+1} are the temperatures at neighboring points, while r_j, r_{j-1}, and r_{j+1} are the radial locations of each point, respectively. Now define a control volume that the face of the control volume rr_j is located between r_{j-1} and r_j, and another face rr_{j+1} is located between r_j and r_{j+1}. Then Δr is the distance between the two faces. Therefore, based on the Eq. 2.8 to 2.10, the term ∇T in Eq. 3.19 can be simply discretized as follow in terms of the control volume which is from r_j to r_{j+1}:

$$\frac{\partial \mathrm{T}}{\partial r} = \frac{T_{j+1} - T_j}{r_{j+1} - r_j} \tag{3.20}$$

Next, integrate over the control volume from rr_j to rr_{j+1}:

$$\frac{\partial}{\partial r}\left(\frac{\partial \mathrm{T}}{\partial r}\right) = \frac{1}{rr_{j+1} - rr_j}\left(\frac{T_{j+1} - T_j}{r_{j+1} - r_j} - \frac{T_j - T_{j-1}}{r_j - r_{j-1}}\right) \tag{3.21}$$

Therefore, the heat conduction term can be discretized based on Eq. 3.20 and 3.21:

$$\nabla \cdot \left(k_{eff} \nabla T\right) = \frac{1}{r^2}\frac{\partial}{\partial r}\left(r^2 k_{eff}\frac{\partial T}{\partial r}\right)$$
$$= k_{eff} \cdot \left[\frac{rr_{j+1}^2}{r_j^2\left(rr_{j+1} - rr_j\right)} \cdot \frac{T_{j+1} - T_j}{r_{j+1} - r_j} - \frac{rr_j^2}{r_j^2\left(rr_{j+1} - rr_j\right)} \cdot \frac{T_j - T_{j-1}}{r_j - r_{j-1}}\right] \tag{3.22}$$

Similarly, the heat convection term can also apply the finite volume method to discretize the ∇T term. Moreover, the product of the convective flux per volume $\boldsymbol{u}$ and the gas density inside of the particle ρ is the total convective flux N_{tot}. The variable ρ at every position inside of the particle can be expressed following the ideal gas law:

$$\rho_j = \frac{P_j}{R \cdot T_j} \tag{3.23}$$

R is the gas constant, which the value can be seen as a constant in the model, 286.9 *J/kg-K*. On the other hand, Darcy's Law is applied for determining the convective flux per volume $\boldsymbol{u}$ inside of the porous particle:

$$\boldsymbol{u} = -\frac{B_0}{\mu}\nabla P \tag{3.24}$$

In Eq. 3.24, B_0 is the permeability of the coal, which depends on the porosity and average pore size, and μ is the viscosity of the gas, which is assumed as a constant in this model. Thus the convection term can be discretized based on the finite volume method:

$$\rho_j c_p \boldsymbol{u} \cdot \nabla T = \frac{rr_{j+1}^2}{r_j^2\left(rr_{j+1} - rr_j\right)} \cdot c_p \cdot N_{tot\,j+1} \cdot T_{j+1} - \frac{rr_j^2}{r_j^2\left(rr_{j+1} - rr_j\right)} \cdot c_p \cdot N_{tot\,j} \cdot T_j \tag{3.25}$$

P_j in Eq. 3.23 and ∇P in Eq. 3.24 represent the variable of pressure and the pressure gradient inside of the particle. Conservation of mass is applied to solve the pressure at grid points inside of the particle:[7,25]

$$\frac{d\rho}{dt} + \frac{1}{r^2}\frac{\partial}{\partial r}(r^2 \rho \boldsymbol{u}) = H\frac{\partial \rho}{\partial t} \tag{3.26}$$

Using the ideal gas law and basic differentiation rules to rearrange the equation, and applying the finite volume method, the discretization of the mass conservation equation in terms of pressure can be derived:

$$\frac{dP}{dt} = \frac{P}{R_{mix}} \cdot \frac{dR_{mix}}{dt} + \frac{P}{T} \cdot \frac{dT}{dt} - R_{mix} \cdot T \cdot \frac{B_0}{\mu} \cdot \rho_{gas} \cdot \left(\frac{rr_{j+1}^2}{r_j^2 (rr_{j+1} - rr_j)} \cdot \frac{P_{j+1} - P_j}{r_{j+1} - r_j} - \frac{rr_j^2}{r_j^2 (rr_{j+1} - rr_j)} \cdot \frac{P_j - P_{j-1}}{r_j - r_{j-1}} \right) + H \frac{\partial \rho}{\partial t} \tag{3.27}$$

where R_{mix} is the gas constant of mixture, which is also assumed as a constant in this model and variable ρ_{gas} is the gas density inside of the particle, which is calculated using Eq. 3.23.

In terms of the heat of reaction, the term $d\rho/dt$ describes the change of coal density during the pyrolysis. It is clear that the density of coal decreases with the decomposition of the coal structure and the escape of volatiles. The density change can be calculated through the CPD model. During the process of pyrolysis, the original coal particle is decomposed and releases tar and light gas. Therefore, the density change can be related to the rate of change of tar and light gas:

$$\frac{d\rho}{dt} = -\rho_0 \cdot \left(\frac{df_{tar}}{dt} + \frac{df_{gas}}{dt} \right) \tag{3.28}$$

A half control volume is applied here to set the boundary condition for the temperature equation. For Eq. 3.19, the boundary temperature or heat flux is necessary for solving the differential equation. But generally, we have to construct an additional equation for getting the boundary temperature because the boundary temperature is not given exactly for convective boundary conditions. Therefore, based on the finite volume method, a half control volume can be used only on one side of the grid point to integrate the differential

equation. Fig. 3-3 shows the half control volume near the boundary.

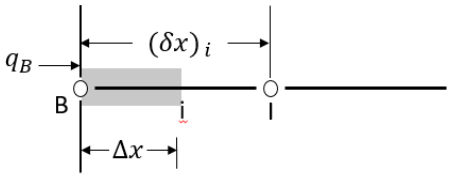

Figure 3-3. Half control volume near the boundary

The gray part is the half control volume. q_B is the boundary heat flux, which can be calculated in terms of a heat transfer coefficient *h* and a surrounding fluid temperature T_f:

$$q_B = h\left(T_f - T_B\right) \tag{3.29}$$

Therefore, using the finite volume method to integrate over this half control volume, the boundary temperature T_B can be evaluated:

$$\left(\rho c_p\right)_{eff} \frac{\partial T_B}{\partial t} = \left[\frac{rr_{j+1}^2}{r_j^2\left(rr_{j+1} - rr_j\right)} \cdot h \cdot \left(T_f - T_B\right) - k_{eff} \cdot \frac{rr_j^2}{r_j^2\left(rr_{j+1} - rr_j\right)} \cdot \frac{T_B - T_{j-1}}{r_j - r_{j-1}}\right] \tag{3.30}$$

After the analysis of every term of the right hand side of Eq.3.19, the non-linear energy equation has been successfully transformed to an algebraic equation, which can be solved mathematically by numerical methods. Table 3-1 shows the necessary properties based on the nature of the coal particle used to get the temperature profile.

Table 3-1. Parameters used to calculate the temperature profile.

Notation	Definition	Value	Unit
$c_{p,coal}$	Specific heat capacity of coal	1380	*J/kg-K*
$c_{p,air}$	Specific heat capacity of air	1080	*J/kg-K*
k_{eff}	Thermal conductivity coefficient of coal	0.4	
R_{air}	Gas constant of air	286.9	*J/kg-K*
ρ_{eff}	Density of lignite particle	833	kg/m^3

E. CPD Model with Improved VLE

The existing VLE model applies a time-lagging method to calculate the partitioning of tar and gas species (or fragments) from the "feed" generated by decomposition of the original macromolecular structure. The generation of tar and gas in the *last* time step is combined with the metaplast that has accumulated from all previous time steps to calculate the moles of fragment *i* per cluster before vapor-liquid equilibrium, f_i.[22] This method has a disadvantage in that the equations themselves depend on the numerical time step, and Fig. 3-4 shows the effect of time step on CPD model.[22]

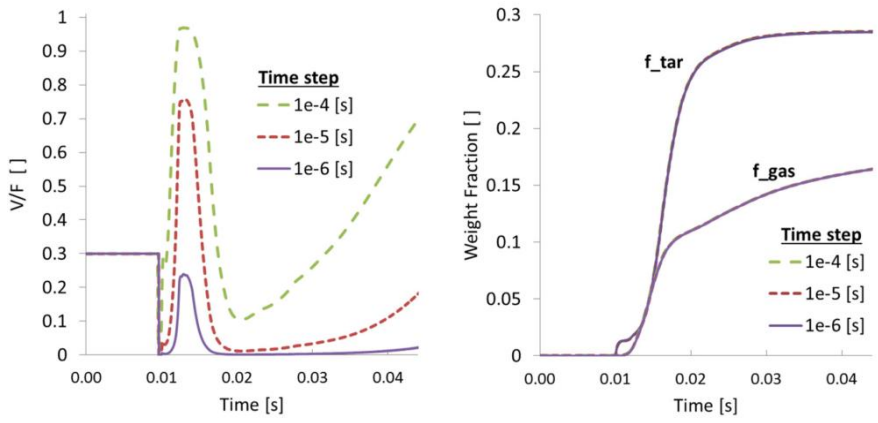

Figure 3-4. The effect of time step on CPD model

It is obvious that even though different time step does not have a significant effect on the mass fraction on tar and gas when large fragment lumps are used, it indeed has a big influence on the fraction of total vapor (*V/F*). With the increase of time step size, the *V/F* increases, which means the *V/F* is highly time-step dependence. This phenomenon could lead to the inaccurate simulation of the pyrolysis when many discrete species are present. So, an improved CPD model with the rate-based VLE method will be developed instead of the "previous-time-step-based" VLE method. The goal of the improved model is to eliminate the time-step dependence and get the more accurate result. Fig. 3-5 shows more details about this improved method.

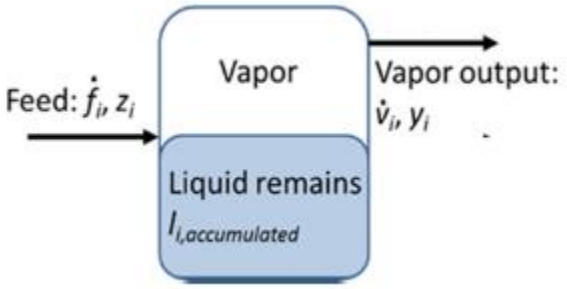

Figure 3-5. Vapor and liquid phase in the "Flash vessel"

Different species in the coal particle are partitioned into two different phases: some species vaporize and go out of the particle and others remains in the particle as liquid. Therefore, a "continuous flash vessel" analogy is used to analyze the pyrolysis behavior. During this process, applying the mass balance equation for every species, the molar flow rate into the system is equal to the molar flow rate out of the system:[22]

$$\frac{dL^*}{dt} + \frac{dV}{dt} = \dot{F} - \dot{V} - k_{cross} \cdot L^* \tag{3.31}$$

where $\dot{F}$ and $\dot{V}$ are the total flow rate at which the fragments are generated and the vapor flow rate of species out of the particle, respectively. And L^* represents the liquid remains in the vessel. Moreover, V and k_{cross} represent the volume of the vapor and the Arrhenius rate constant, which are given be:[5]

$$V = \frac{P}{n_v \bar{R} T} \tag{3.32}$$

$$k_{cross} = A_{cross} \exp\left(\frac{-E_{cross}}{\bar{R}T}\right) \tag{3.33}$$

The value of A_{cross} and E_{cross} depends on the characteristics of coal particle. From Eq. 3.31, the differential equation of species *i* can be derived through inserting the Eq. 2.2, 2.3, and 2.6 into Eq. 3.31 and rearranging it using the chain rule to give:

$$\frac{dx_i}{dt} = \left[\frac{(z_i - x_i)\dot{F}}{L^* + V \cdot K_i} + \frac{x_i(1 - K_i)\dot{V}}{L^* + V \cdot K_i} - \frac{V \cdot x_i}{L^* + V \cdot K_i} \cdot \frac{dK_i}{dt} + \frac{x_i(1 - K_i)}{L^* + V \cdot K_i}\frac{dV}{dt}\right] \tag{3.34}$$

This is the expression for the mole fraction of each species in the liquid phase. Now applying the VLE method, the Eq. 2.6 can be updated based on the size of fragment:[5]

$$y_n = K_n \cdot x_n \tag{3.35}$$

$$K_n = \frac{P_n^v}{P} = \frac{\alpha \cdot exp\left(-\beta \cdot m_{frag,n}^{\gamma}/T\right)}{P} \tag{3.36}$$

where the parameter K_n is the resulting correlation for coal tars developed by Unger and Suuberg.[5] α, β and γ are parameters which depends on the characteristics of coal particle, and *M* is the molecular weight of fragment *n*. Moreover, in terms of different species, Eq.

3.35 and 3.36 can not only use for getting the K_n and x_n for every fragments or each discrete species.

Next, in terms of z_i in Eq. 3.34, it represents the number fraction of different size of fragments of the feed entering the flash vessel. Moreover, the number fraction of the *feed* can be divided into two parts: the light gas and tar/metaplast. Furthermore, the sum of the number of fragments of light gas and tar/metaplast is equal to the total flow rate of generated fragments, which is $\dot{F}$.

$$\dot{F} = \sum_{i=1}^{n} z_i' + z_{gas}' \tag{3.37}$$

where z_i' is the mole of each fragment of tar/metaplast and z_{gas}' is the mole of each fragment of light gas. Both of them can be derived from the following differential equation:[22]

$$z_i' = \frac{d}{dt}\left(\frac{Q_i}{m_{total}}\right) \tag{3.38}$$

$$z_{gas}' = \frac{d}{dt}\left(\frac{m_{gas}/MW_{gas}}{m_{total}}\right) \tag{3.39}$$

where the Q_i is the number of fragments of size i per cluster in the CPD model, and it depends on the percolation theory and use the parameters of *s, τ,* and *p*. Also, m_{gas} is the mass of gas release per cluster:[5]

$$Q_n = b_n^{site} p^s (1-p)^\tau \tag{3.40}$$

$$b_n^{site} = \frac{1}{n} \cdot \frac{\sigma+1}{s+\tau} \cdot \frac{\Gamma(s+\tau+1)}{\Gamma(s+1)\Gamma(\tau+1)} \tag{3.41}$$

$$m_{gas} = m_b \cdot g \cdot (\sigma+1)/4 \tag{3.42}$$

Therefore, the number fraction of each fragment of tar/metaplast and light gas can be derived, which is required in Eq. (3.34):

$$z_i = z_i'/\dot{F} \tag{3.43}$$

$$z_{gas} = z_{gas}'/\dot{F} \tag{3.44}$$

Now, the last unknown variable of source term of Eq. 3.34 is the total flow rate of vapor species out of the particle, $\dot{V}$. This is determined from the constraint that all gas-phase mole fractions adds to unity, which means $\sum y_i = 1$.[32] This constraint produces a non-linear, index-2 DAE system.[20]

Furthermore, Section C has discussed the relationship between the number fraction of fragments, z_i, and the number fraction of discrete species at every time step, $w_j(t)$. Therefore, z_i can be replaced by $w_j(t)$ and the ultimate goal has been achieved, which is that the governing equation (Eq. 3.34) can be solved for the mole fraction of discrete species in the liquid phase at all times. Table 3-2 shows more parameters based on the nature of the coal particle used in CPD model and the VLE method.[5]

Table 3-2. Parameters used in CPD model and VLE method

Notation	Definition	Value	Unit
A_b	Bridge scission frequency factor	2.6×10^{15}	*1/s*
E_b	Bridge scission activation energy	55400	*cal/mol*
σ_b	Standard deviation for distribute E_b	1800	*cal/mol*
ρ	Composite rate constant k_δ/k_c	0.9	
E_{cross}	Activation energy for cross-linking in coal	65000	*cal/mol*
A_{cross}	Pre-exponential factor for cross-linking in coal	3×10^{15}	*1/s*
$\bar{R}$	Gas constant in CPD model	1.987	*cal/K·mol*
α	Coefficient in vapor pressure correlation	87060	
β	Coefficient in vapor pressure correlation	299	
γ	Coefficient in vapor pressure correlation	0.59	
m_a	Average mass of the fused ring site	165.8	*g*
m_b	Mass of the bridges	44	*g*

F. Initial Condition for Improved VLE Model

Like the temperature differential equation, we also have to know the boundary condition for improved CPD model. In terms of labile bridge and charred bridge, the initial value of them based on the characteristics of coal particle are the boundary condition of the equation 3.1 and 3.2. Moreover, the initial condition of mass fraction of cross-linked metaplast and tar can be set as zero because the pyrolysis does not happen at the beginning of the pyrolysis. Last, but not least, the initial condition for discrete species and the accumulated liquid species is more complicated to solve. The improved CPD model can be solved only the initial conditions are consistent because the new VLE sub-model is an

index-2 system of differential algebraic equations (DAEs), which can be expressed as the semi-explicit form in terms of y_i[20]:

$$\frac{dy_i}{dt} = f(y_i, \dot{V})$$
$$0 = g(y_i) \tag{3.45}$$

The "hidden constraint" for the initial conditions can be obtained by differentiating the equation with respect to the variable y_i:

$$0 = g_y \frac{dy}{dx} = g_y f(y, z) \tag{3.46}$$

Then the initial value y_0 and z_0 which can satisfy the system of equation 3.46 are the consistent initial conditions for this index-2 DAEs system.

$$g(y_0) = 0$$
$$g_y(y_0) f(y_0, z_0) = 0 \tag{3.47}$$

Therefore, applying equations 3.45 to the CPD model and after the mathematical transformation, the consistent initial conditions for discrete species and the accumulated liquid species can be calculated from the relations:

$$\sum x_i = 1$$
$$\sum K_i x_i = 1 \tag{3.48}$$
$$K_i \frac{dx_i}{dt} = 0$$

With this, all the ODEs for describing the process of pyrolysis based on the general CPD model and the generation of the species in terms of fragment or discrete species have been introduced. The improved CPD model accounts for heat transfer limitations to simulate the pyrolysis at every position in a large-scale coal particle. Moreover, it can describe the process of vaporization by using the multicomponent vaporization equations described above, which improve the accuracy of existing model due to the elimination of the time dependence. Finally, after incorporating the VLE method and connecting the VLE method and CPD model, this model can predict the generation of the discrete species at every time-step during the process of pyrolysis, which is not possible using the general CPD model.

Chapter IV. Direct Quadrature Method of Moments for Pyrolysis

In Chapter III, an improved CPD model with a new VLE method was introduced and developed to simulate the process of pyrolysis and the generation of discrete species. However, more than 500 hundred of discrete tar species can be generated during pyrolysis, and solving ODEs (3.34) for each species, x_i, is a little complicated and inefficient, which leads to increasing computation time. On the other hand, as section D in Chapter II mentioned, the *distribution* of species $x(\xi)$ at every single time can be described by using the Quadrature Method of Moment (QMoM) or the Direct Quadrature Method of Moment (DQMoM). Therefore, the DQMoM model will be applied to solve for the mole fraction of "lumped" species characterizing the *distribution* of x_i and then a delumping method based on an "integrating factor" is used to obtain the exact mole fraction of each species from "lumped" species at every single time.

The motivation for applying the DQMoM in the CPD model is simplifying the calculation process and improving the computational effectivity. Compared with solving the difficult non-linear differential Eq. 3.34 by specific ODEs solver 500 times, the right hand side of Eq. 3.34 also can be regarded as the source term to be integrated (see Eq. 2.13) and solved by quadrature approximation, which is the main goal of DQMoM.

A. Weights and Nodes

The improved CPD model introduced in Chapter III has developed an accurate way to solve the mole fraction of all discrete species (Eq. 3.34). On the other hand, the DQMoM requires the solution of equations for weights w and nodes ξ of the quadrature approximation, where the definition of w and ξ have been introduced in Chapter II.

Compared with the Eq. 3.34, the mole fraction of species for each fragment x_i and molecular weight of each fragment $m_{frag,n}$ are equivalent with the weight w_i and the nodes ξ_i. Therefore, Eq. 2.11 can be rearranged to a differential equation with regarding the right hand side of Eq. 3.34 as the source term as follow:[26]

$$\frac{dx(\xi;t)}{dt} = S \tag{4.1}$$

Based on the Eq. 2.13 to 2.16, Eq. 4.1 can be rearranged to the following form, which is the linear system of ODEs:[26]

$$(1-k)\sum_{i=1}^{n}\xi_i^k\, a_i + k\sum_{i=1}^{n}\xi_i^{k-1}\, b_i = \bar{S}_k \tag{4.2}$$

where the continuous term $dx(\xi)/dt$ has been replaced by the transport equations for weights and nodes:[26]

$$a_i = \frac{dw_i}{dt};\;\; b_i = \frac{d(w_i\xi_i)}{dt} \tag{4.3}$$

Furthermore, it is clear that the total number of variables a_i and b_i are $2n$, and in order to solve this system of ODEs, $2n^{th}$ equations should be required, which means we use moments $k=0, 1, 2, \ldots, 2n-1$.[15] Then all the equations can be reformed based on the matrix theory. Evaluating the source term vector as described below, we can get the evolution of weights w_i and nodes ξ_i with the time by solving the system of ODEs in Eq. (4.4). [26]

$$\begin{pmatrix} 1 & \cdots & 1 & 0 & \cdots & 0 \\ 0 & \cdots & 0 & 1 & \cdots & 1 \\ -\xi_1^2 & \cdots & -\xi_n^2 & 2\xi_1 & \cdots & 2\xi_n \\ \vdots & \vdots & \vdots & \vdots & \vdots & \vdots \\ -2(1-n)\xi_1^{2n-1} & \cdots & -2(1-n)\xi_n^{2n-1} & (2n-1)\xi_1^{2n-2} & \cdots & (2n-1)\xi_n^{2n-2} \end{pmatrix} \begin{pmatrix} a_1 \\ \vdots \\ a_n \\ b_1 \\ \vdots \\ b_n \end{pmatrix} = \begin{pmatrix} \bar{S}_0 \\ \bar{S}_1 \\ \vdots \\ \vdots \\ \bar{S}_{2n-2} \\ \bar{S}_{2n-1} \end{pmatrix} \tag{4.4}$$

B. Source term

In the DQMoM, the moment transform of the source term $\bar{S}_k$ should be evaluated with a quadrature approximation. From Eq. 3.34 and Eq. 4.1, the source term S for the continuous distribution is:

$$S(\xi) = \frac{\big(z(\xi) - x(\xi)\big)\dot{F}}{L^* + V \cdot K(\xi)} + \frac{x(\xi)\big(1 - K(\xi)\big)\dot{V}}{L^* + V \cdot K(\xi)} - \frac{V \cdot x(\xi)}{L^* + V \cdot K(\xi)} \cdot \frac{dK(\xi)}{dt} + \frac{x(\xi)\big(1 - K(\xi)\big)}{L^* + V \cdot K(\xi)} \frac{dV}{dt} \tag{4.5}$$

Next, in terms of source term $\bar{S}_k$ in Eq. 4.2, the quadrature approximation for the source term will be applied to get a relationship between the S and $\bar{S}_k$. The goal of using quadrature approximation is to make the $\bar{S}_k$ closed with the function of weight w_i and the nodes ξ_i . Therefore, the quadrature approximation of $\bar{S}_k$ can be derived based on the QMoM theory introduced in Eq. 2.13:

$$\bar{S}_k = \int_0^{+\infty} \xi^k \left[\frac{\big(z(\xi) - x(\xi)\big)\dot{F}}{L^* + V \cdot K(\xi)} + \frac{x(\xi)\big(1 - K(\xi)\big)\dot{V}}{L^* + V \cdot K(\xi)} - \frac{V \cdot x(\xi)}{L^* + V \cdot K(\xi)} \cdot \frac{dK(\xi)}{dt} + \frac{x(\xi)\big(1 - K(\xi)\big)}{L^* + V \cdot K(\xi)} \frac{dV}{dt} \right] d\xi \tag{4.6}$$

Now Eq. 4.6 can be divided into several part to match the form of Eq. 2.13, and get the interpolation formula of each part. For example, after multiply ξ^k by every term of right hand side, the second integral term from Eq. 4.6 can be extracted and got its interpolation formula as the following steps. Defining $G(\xi)$ for convenience:

$$G(\xi) = \frac{\big(1 - K(\xi)\big)}{L^* + V \cdot K(\xi)} \tag{4.7}$$

Then the second integral term of the Eq. 4.6 can be simplified through $G(\xi)$ and replacing $x(\xi)$ by a summation which is introduced as Eq. 2.14:

$$\int_0^\infty \xi^k \frac{x(\xi)\big(1 - K(\xi)\big)\dot{V}}{L^* + V \cdot K(\xi)} d\xi = \dot{V} \int_0^\infty \xi^k G(\xi) \sum_{\alpha=1}^{n} w_\alpha \delta[\xi - \xi_\alpha]\, d\xi \tag{4.8}$$

Therefore, the integral form in Eq. 4.8 can be transformed into a weighted summation of *n* terms through the Gaussian quadrature based on Eq. 2.18.

$$\dot{V} \int_0^\infty \xi^k G(\xi) \sum_{\alpha=1}^{n} w_\alpha \delta[\xi - \xi_\alpha]\, d\xi = \dot{V} \sum_{\alpha=1}^{n} \xi_\alpha^k w_\alpha G(\xi) \tag{4.9}$$

Where the variables $\dot{V}$ in Eq. 4.9 represents the total flow of vapor species out of the particle in DQMoM model. The equation of it is similar to the constraint in the improved CPD model, and it is calculated by the constraint with the weight:

$$\sum_{\alpha=1}^{n} y_\alpha = \sum_{\alpha=1}^{n} w_\alpha K_\alpha = 1 \tag{4.10}$$

The accuracy of this equation is quantified by its degree of accuracy and the order of the polynomial of integrand functions. The interpolation formula is exact when the order of polynomial is smaller than or equal to the degree of accuracy. So in terms of the integrand function in Eq. 4.8, the minimum degree of accuracy is three if three nodes are used. The higher accuracy the interpolation function has, the more accurate result we can get compared with the exact value.

Similarly, we can use the same method to transform other terms in Eq. 4.6 to a summation of *n* terms by assuming other *G* function for convenience:

$$G_1(\xi) = \frac{1}{L^* + V \cdot K(\xi)} \tag{4.11}$$

$$G_2(\xi) = \frac{1}{L^* + V \cdot K(\xi)} \cdot \frac{dK(\xi)}{dt} \tag{4.12}$$

Then the other terms of the right hand side in Eq. 4.6 can be transformed:

$$\int_0^\infty \xi^k \frac{-x(\xi)\dot{F}}{L^* + V \cdot K(\xi)} d\xi = -\dot{F} \sum_{\alpha=1}^{n} \xi_\alpha^k w_\alpha G_1(\xi) \tag{4.13}$$

$$-\int_0^\infty \xi^k \frac{Vx(\xi)}{L^* + V \cdot K(\xi)} \frac{dK(\xi)}{dt} d\xi = -V \sum_{\alpha=1}^{n} \xi_\alpha^k w_\alpha G_2(\xi) \tag{4.14}$$

$$\int_0^\infty \xi^k \frac{x(\xi)\big(1 - K(\xi)\big)}{L^* + V \cdot K(\xi)} \frac{dV}{dt} d\xi = \frac{dV}{dt} \sum_{\alpha=1}^{n} \xi_\alpha^k w_\alpha G(\xi) \tag{4.15}$$

Now, all the integral terms including $x(\xi)$ have been transformed. However, the term with $z(\xi)$ is not transformed because the feed distribution, $z(\xi)$, is just an externally imposed source term due to the pyrolysis chemistry; it does not to be solved as part of the

VLE method. Moreover, there is no need to use the same w_α and ξ_α in $z(\xi)$ because it is just a constant after the term with $z(\xi)$ get integrated. Thus, to transform this term to the simple summation form, an effective way is applying the full details of discrete species on $z(\xi)$ and using the same method introduced in Chapter III to get the mole fraction of each species $w_j(t)$ at every time step.

$$\int_0^\infty \xi^k \frac{z(\xi)\dot{F}}{L^* + V \cdot K(\xi)} d\xi = \dot{F} \sum_{j=1}^{N} \xi_j^k w_j(t) G_1(\xi) \tag{4.16}$$

In this equation, *N* is the total number of the discrete species, and ξ_j^k is all the molecular weights of feed species produced by bridge breaking. Therefore, the source term $\bar{S}_k$ has been fully transformed to a summation and is now closed and we can insert it into Eq. 4.4 to solve the variables vector and derived the simple differential equation for w_i. Then the mole fraction of species for every node can be easily solved.

As in Chapter III, consistent initial conditions are also very significant for solving DQMoM model. Recalling the consistent initial conditions for index-2 DAEs system introduced in Chapter III, based on the result shown in Eq. 3.48, we can get the initial conditions for w_i:

$$\begin{aligned} \sum w_i &= 1 \\ \sum K_i w_i &= 1 \end{aligned} \tag{4.17}$$

Moreover, Eq. 3.46 can be rearranged based on the weight w_i and the weighted nodes $w_i\xi_i$ separately. For the weight w_i, we can get that:

$$\frac{dg}{dw_i} \cdot \frac{dw_i}{dt} = 0 \tag{4.18}$$

Similarly, for the weighted abscissas (nodes) $w_i\xi_i$, the consistent initial condition is:

$$\frac{dg}{d(w_i\xi_i)} \cdot \frac{d(w_i\xi_i)}{dt} = 0 \tag{4.19}$$

Then the second equation in equation system 4.17 can be inserted into Eq. 4.18 and 4.19 instead of function g and the consistent initial conditions can be derived after the mathematical transformation:

$$\begin{gathered} K_i \cdot \frac{dw_i}{dt} = 0 \\ \frac{-(K_i w_i) \cdot \beta \cdot \gamma \cdot (w_i\xi_i)^{\gamma-1}}{T w_i^{\gamma}} \frac{d(w_i\xi_i)}{dt} = 0 \end{gathered} \tag{4.20}$$

These four equations in 4.17 and 4.20 are the consistent initial conditions for DQMoM model. Using these equations can get the initial values of weight and nodes which are required to solve the ODEs in DQMoM model.

C. Delumping

While the full discrete version of the improved CPD model solves for every x_i, DQMoM solves for several nodes and weight to represent the evolving distribution of $x(\xi)$. The weights, w_i, can be thought of as the mole fractions for each node (molecular weight), in other word, for each "lumped" species. So, if we want to know the generation of *discrete*

tar species at every single time, it is necessary to "delump" the discrete species from the lumped solution.

After the mole fraction for every node is solved by DQMoM model, we know w_i and ξ_i with time, other state variables such as $\dot{V}$, as well as all other non-state variables, including $\dot{F}_{tot}, L^*, V$ and K. All of these variables are used for solving Eq. 3.34 for discrete species. The value of all these other variables obtained from DQMoM should be very close to the result from the full discrete version of the improved CPD model.

Recall, Eq. 3.34, is a differential equation for x_i. Moreover, it can be rearranged by combining all the term of x_i terms into one:

$$\frac{dx_i}{dt} = \frac{z_i \dot{F}}{L^* + V \cdot K_i} + x_i \left[\frac{-\dot{F}}{L^* + V \cdot K_i} - \frac{(1 - K_i)\dot{V}}{L^* + V \cdot K_i} - \frac{V \cdot dK_i/dt}{L^* + V \cdot K_i} + \frac{(1 - K_i) \cdot dV/dt}{L^* + V \cdot K_i} \right] \quad (4.21)$$

Unlike using the ODE solver to solve this nonlinear equation as in Chapter III, the difficult nonlinear term $\dot{V}$ has been solved through the DQMoM method and now the equation is linear. Therefore, the integrating factor method will be applied to solve this equation once all the other terms are known functions of time after the DQMoM solution. In general, if an ODE can be expressed in the form:

$$\frac{dx}{dt} + P(t)x = Q(t) \quad (4.22)$$

where the variable *y* is a function of *x*. Then the integral factor *u(x)* can be derived and used to solve the Eq. 4.21:

$$u(t) = \exp(\int P(t)dt) \quad (4.23)$$

$$x = \frac{\int u(t)Q(t)dt + C}{u(t)} \tag{4.24}$$

where *C* is determined by the initial value x_0 at *t* equals t_0. Therefore, compared with Eq. 4.20 and 4.21, equation 4.20 can be solved by the integrating factor method. Moreover, internal variables z_i should be replaced by $w_j(t)$ to get the result for discrete species. And the initial value for discrete species at *t=0* is necessary. It is easy to prove that at *t=0*, the value of *C* equals to the initial value of each discrete species.

In summary, all discrete mole fraction at all times can be calculated through the DQMoM model and a subsequent delumping method. Compared with the full discrete model in Chapter III, both can get the distribution of discrete species. However, the DQMoM with delumping model can save the computational time because it reduces the number of ODEs compared with the full discrete version of the model. Furthermore, DQMoM has been proven to be quite accurate in general, and this will be shown to apply here as well in Chapter V. Therefore, solving the improved CPD model using DQMoM + delumping can get almost the same results as the full discrete species model, while reducing computational expense.

Chapter V. Results and Discussion

This chapter presents results from the improved CPD model, which incorporates the transient VLE sub-model, using both the full discrete species model and the DQMoM model with delumping to compute the detailed species distribution with reduced computation time. In the MATLAB code, all of the ordinary differential equations in these two models are solved by the ODEs solver "IDA", which is a C solver applied in MATLAB via "mex" function. These two models, the full discrete species model and the DQMoM + Delumping model, are used to simulate pyrolysis with various particle sizes and pyrolysis temperatures. The evolution of chemical structural properties, tar, gas and char yields, and the capability of the model to simulate discrete tar species will be demonstrated and discussed. Also, the two versions of the improved CPD model will be compared to each other to demonstrate the accuracy of DQMoM + Delumping model, which can save significant computational time with respect to the full discrete species model.

A. Temperature Profile

The temperature profile within a particle undergoing pyrolysis can be obtained by solving the equation of thermal energy conservation, which has been discretized using the finite volume method. Based on industrial interest in slow pyrolysis for chemical production, Wang introduced a temperature profile for low temperature pyrolysis of lignite in an industrial furnace,[28] and an experimental investigation of lignite pyrolysis at higher temperature has been developed by Paprika.[29] Therefore, two different temperature profiles, with maximum temperatures of are 785K and 873K, are used into this study to examine the dependence of the pyrolysis model on temperature. Fig. 5-1 shows the imposed

transient boundary temperature of 0.8mm radius of particle. It is noticeable that this is just a zoom in to short times, since the temperature is constant after 7.5 seconds.

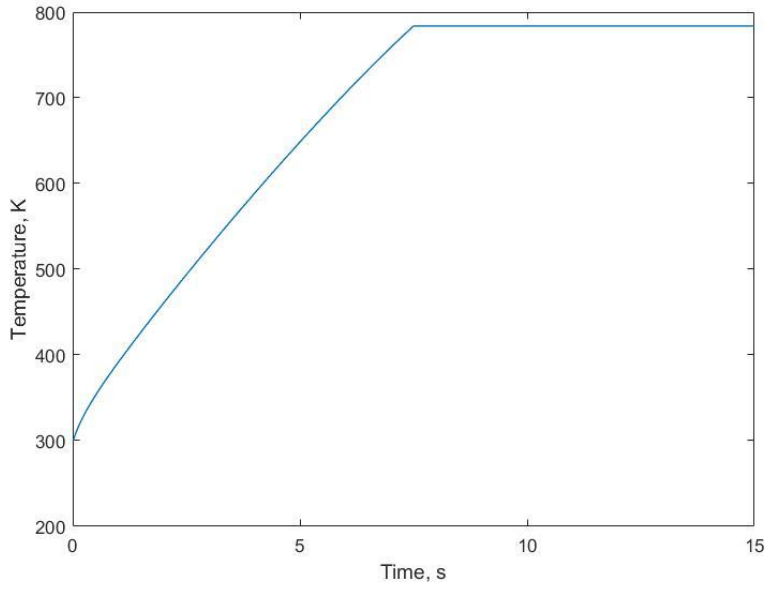

Figure 5-1. Boundary condition temperature profile of 0.8mm radius particle

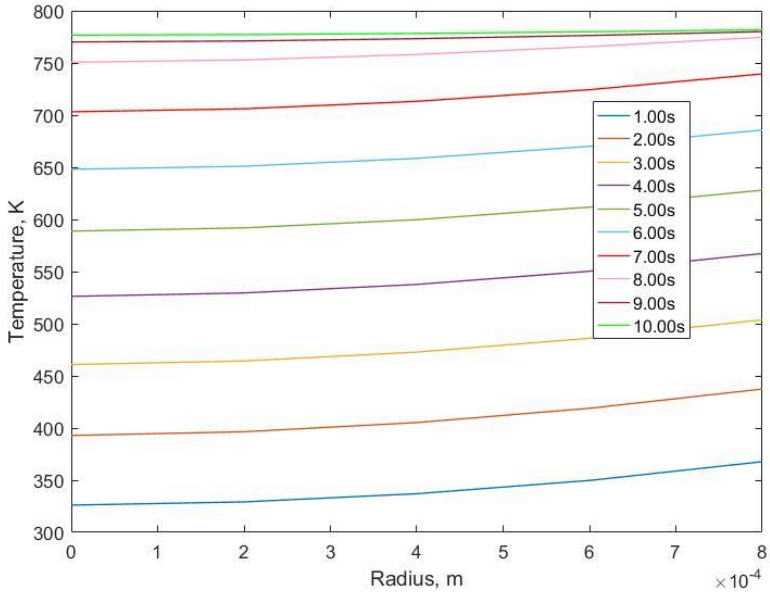

Figure 5-2. Temperature profile of 0.8 mm radius of particle versus different positions inside of the particle at various times.

Fig. 5-2 shows the temperature profile within a 0.8 mm radius particle at various times. The temperature reaches its maximum value, 785K, at every position within 10 seconds. The temperature inside the particle decreases from the surface to the center of the particle, which is reasonable based on the theory of heat transfer. The temperature difference between the center and surface of the particle is a bit below 50K and the difference between surface and center temperatures becomes smaller and smaller as time goes by. However, for a larger coal particle, for example, a particle with radius 4.5 mm, the temperature gradient across the particle will become much larger, and the time required for the entire particle to reach the maximum temperature will increase. This can be seen in Figs. 5-3 and 5-4.

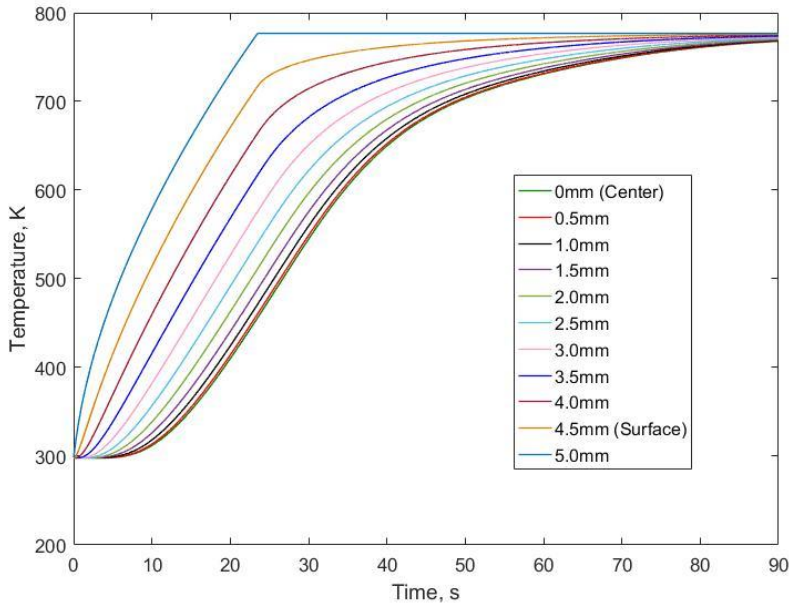

Figure 5-3. Temperature profile of 4.5mm radius of particle at 785K

Figures 5-3 shows the **t**emperature profile of 4.5 mm radius of particle at 785K. The temperature at the center of the particle increases much more slowly than for smaller

particles, and the temperature difference between the center and surface of the particle before 25 seconds is 150K larger than for smaller particles. Figures 5-4 show temperature profiles for the particle from 10 seconds to 90 seconds. The distribution of temperature is different from the smaller particle, and the difference between the center and surface is a bit larger than smaller particle, but it also decreases as time goes by. This section demonstrates the model's capability to simulate temperature gradients occurring in coal particles during pyrolysis. This capability will be used to evaluate whether temperature gradients affect the yields of gas and tar and the production of particular tar species.

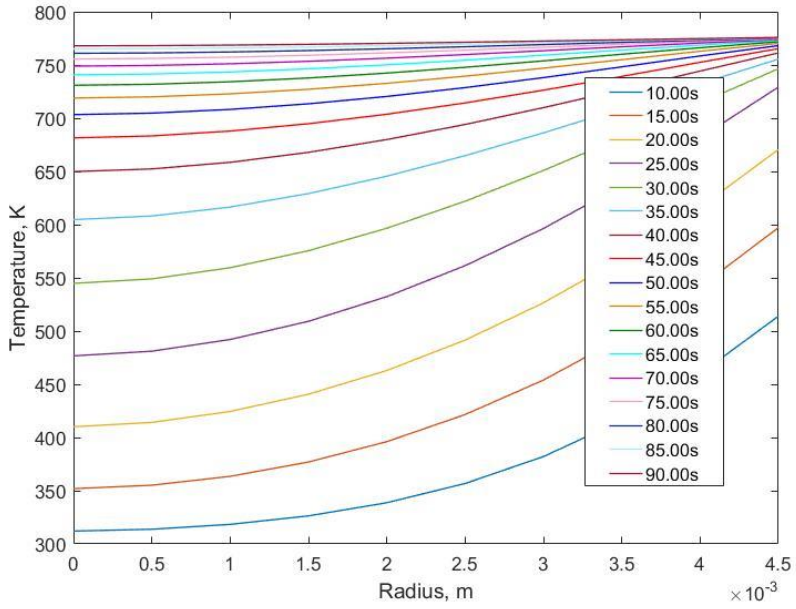

Figure 5-4. Temperature profile of 4.5 mm radius of particle versus different positions inside of the particle at various times

B. CPD and Chemical Properties

In this section, the evolution of the coal chemical properties will be examined. Based on the CPD model, we can obtain the concentration of labile bridges *L*, charred

bridge c, the mass fraction of tar, f_{tar}, the mass fraction of light gas, f_{gas}, and the mass fraction of solid, f_{solid}. The following figures show the change of properties versus time at different position for the 0.8 mm radius particle with the temperature profile shown in Fig. 5-1.

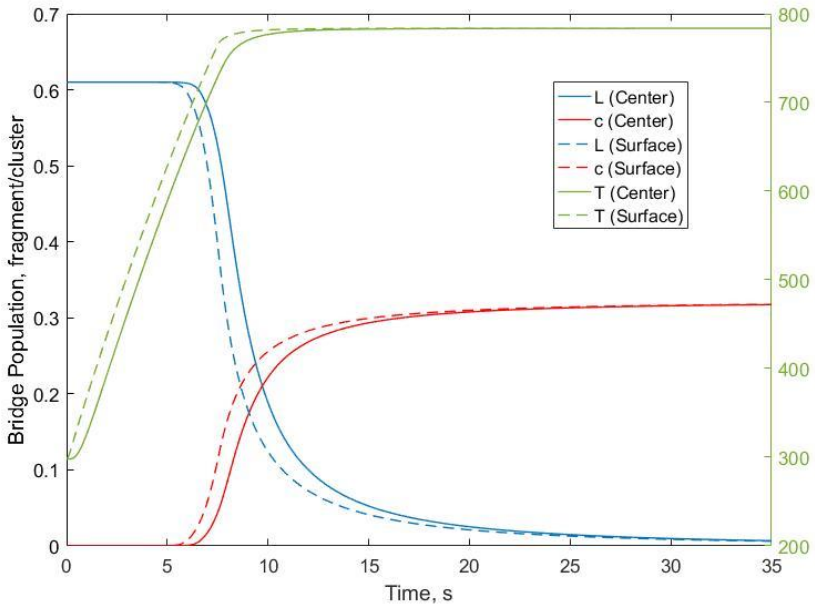

Figure 5-5. The change of labile and charred bridge versus time at the center and surface of the 0.8mm radius of coal particle

Recall the characteristics of the CPD model introduced in Chapter III: as temperature increases, the unstable labile bridges can break in two ways, and can be stabilized to form a char bridge via one pathway.[5] As seen in Fig. 5-5, at the initial time there are labile bridges and no charred bridges. As the temperature increases, at approximately 650 K, the number of labile bridges begins to decrease, with the increase of charred bridges occurring simultaneously. This represents the beginning of pyrolysis. Also,

it is clear that, even for this relatively small particle, pyrolysis begins at the surface of the particle first because temperature rises faster at the surface of the particle than at the center.

However, the final value of the population of labile and charred bridges will be same for different locations in the particle, as long as all locations achieve the same maximum temperature. Fig. 5-6 proves this, using a different radius particle and the local temperature evolution shown in Fig. 5-3. The reason for this is that no matter what the position of the particle is, the ratio of rates k_δ/k_c, which is introduced in Section D of Chapter III, is a constant, which leads to the same final state of the particle after the pyrolysis finishes.

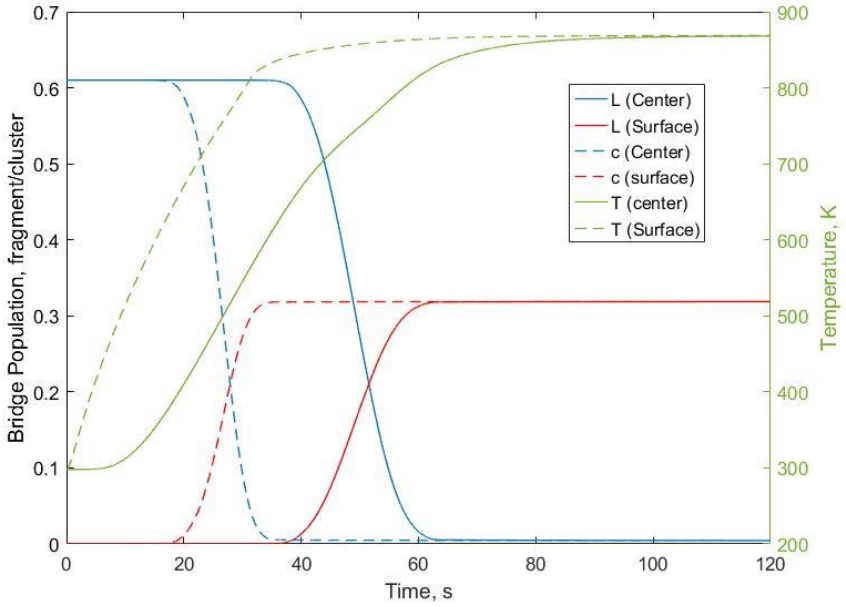

Figure 5-6. The change of labile and charred bridge versus time at the center and surface of the 4.5mm radius of coal particle

Fig. 5-7 shows the change of mass fraction of tar, gas and solid versus time at different positions within the 0.8 mm radius particle at 785K. The mass fraction of tar and

gas are calculated by the Eq. 3.15 and 3.16, and the mass fraction of solid is obtained from the sum of all the fractions being equal to one.

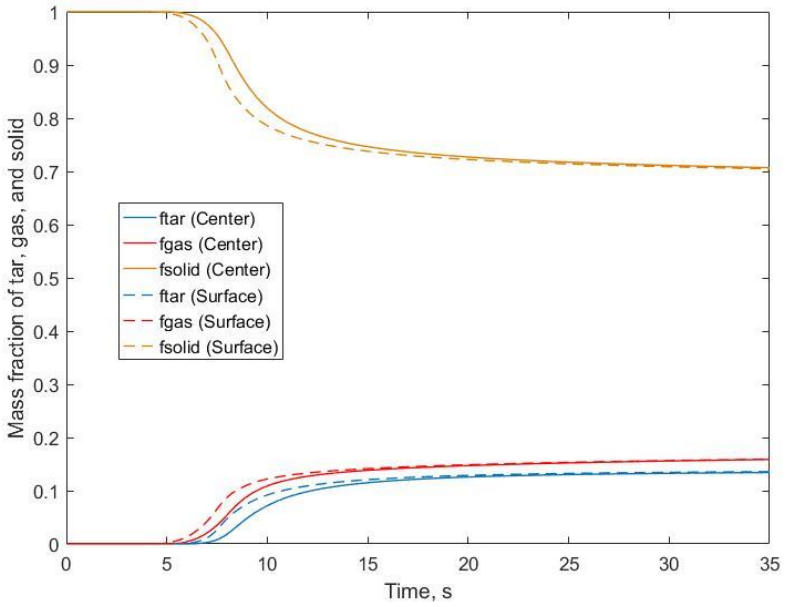

Figure 5-7. The change of mass fraction of tar, gas and solid versus time at the center and surface of the 0.8mm radius of coal particle at 785K

As Chapter III mentioned, the general CPD model can describe the initial thermal decomposition of coal into different volatiles, including light gases and heavier fragments, and account for partitioning of the fragments into vapor (tar) and liquid (which eventually forms char).[5] Fig. 5-7 illustrates this and also matches Fig. 5-6 in that the mass fraction of tar and gas increases first at the surface of the coal particle, where the bridges break first. The fraction of char can be converted to an equation for the density of coal particle, whose evolution is shown in Fig. 5-8. Also, compared with the mass fraction of tar and gas, the mass fraction of solid remaining in the coal particle is larger, for these conditions.

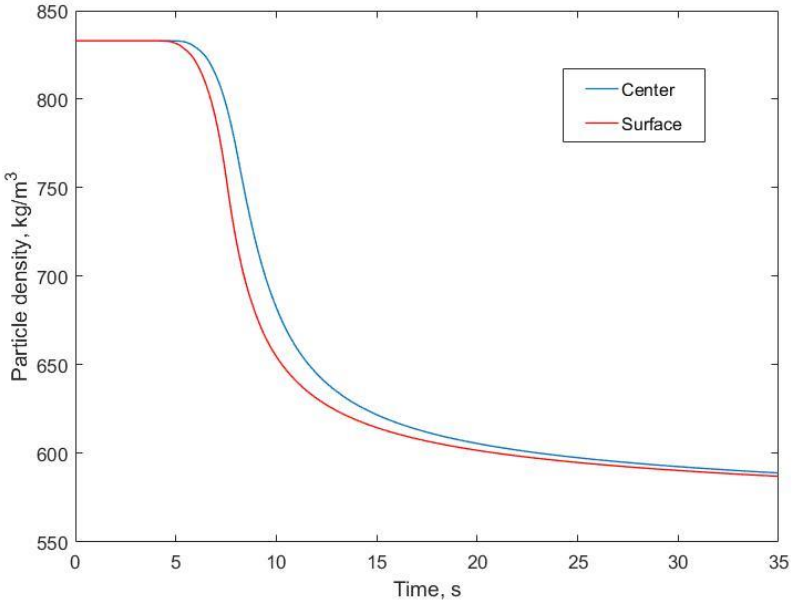

Figure 5-8. The change of density of particle versus time at the center and surface of the 0.8mm radius of coal particle with 785K highest temperature

Figs. 5-9 to 5-12 show the change in chemical properties and yields versus position at various times for the 4.5 mm radius particle with the temperature profile shown in Fig. 5-3. Pyrolysis begins from the surface of the particle and with the time goes by, the pyrolysis for surface of the particle is almost done, while the pyrolysis for near the center of the particle continues. The pyrolysis of the whole particle is almost finished after 90s because the population of labile bridge goes to near the zero, which is shown in Fig. 5-9.

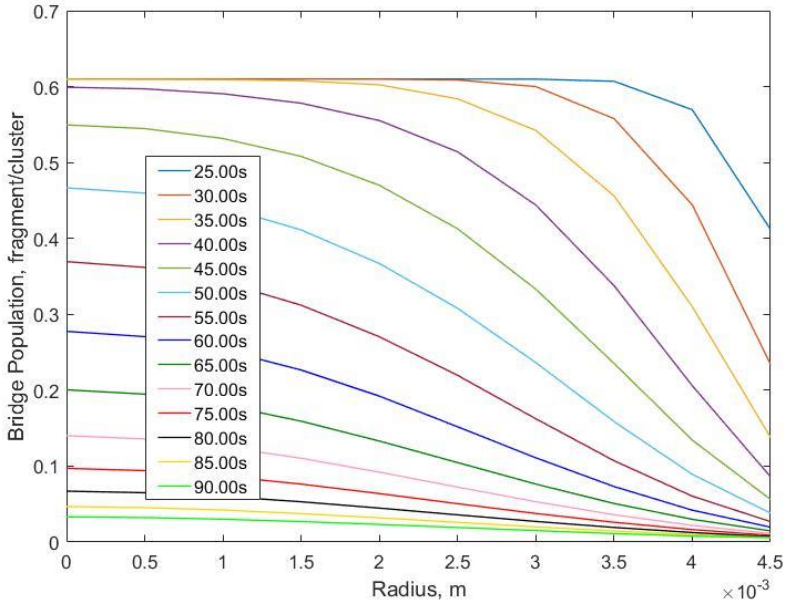

Figure 5-9. The change of labile bridge versus positions at particular time for the 4.5mm radius of coal particle with 785K highest temperature

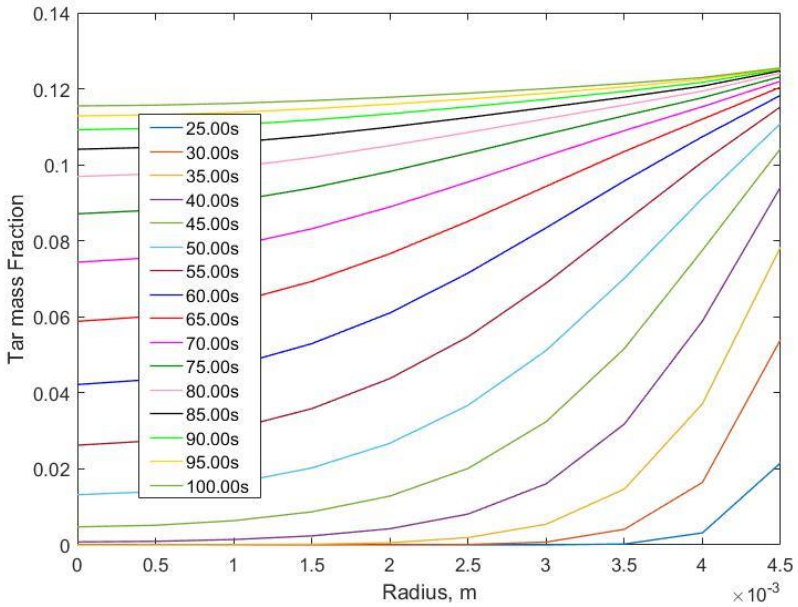

Figure 5-10. The change of mass fraction of tar versus position at particular time for the 4.5mm radius of coal particle with 785K highest temperature

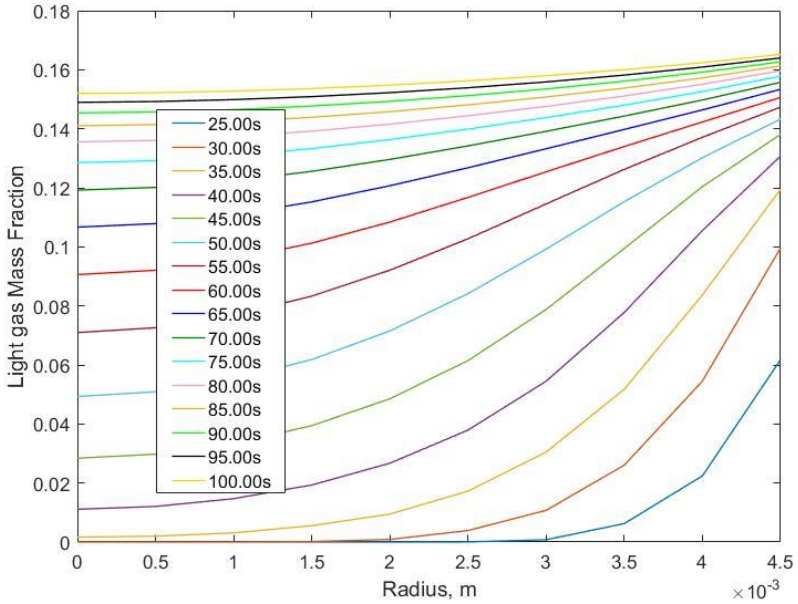

Figure 5-11. The change of mass fraction of gas versus position at particular time for the 4.5mm radius of coal particle with 785K highest temperature

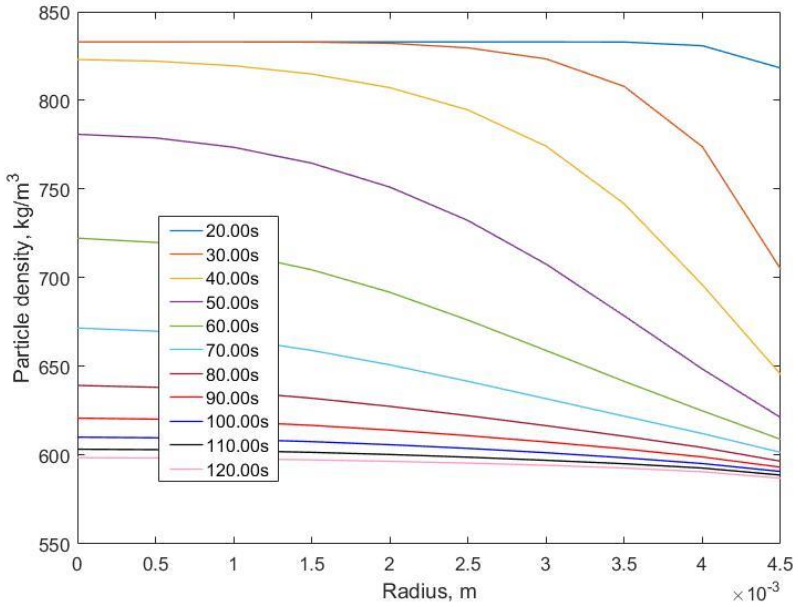

Figure 5-12. The change of density versus positions at particular time for the 4.5mm radius of coal particle with 785K highest temperature

Fig. 5-10 and 5-11 show that the behavior of tar and gas release is similar; it begins at the surface of the particle first, and then the whole particle will release the tar and gas with the process of heat transfer. That leads to the decreasing of density from the surface to the center, which is shown in Fig. 5-12.

While the maximum pyrolysis temperature is the most important parameter, the temperature-time profile also has an influence on the pyrolysis process. If we regard the particle as a point and solve it by using an average temperature, the accuracy of the pyrolysis result for whole particle will decrease. However, if two sizes of coal particles are pyrolyzed in the same boundary temperature, different regions within the particle will be subjected to different temperature-time histories, although the final temperature at each position will be the same. Therefore, it is necessary to resolve large particles spatially to obtain the result for different positions inside of the particle and then to get results for whole particle by numerical integration. Figure 5-13 shows the comparison of the mass fraction of tar, gas and solid at the final time for 0.8mm and 16mm radius of coal particle at 785K. It is clear that at the similar boundary temperature profile, the generation of tar and gas are different for different sizes of particles. What is more, the result proves that the pyrolysis chemistry is related to the particle size, and the particle should be resolved spatially to get the accurate result for pyrolysis.

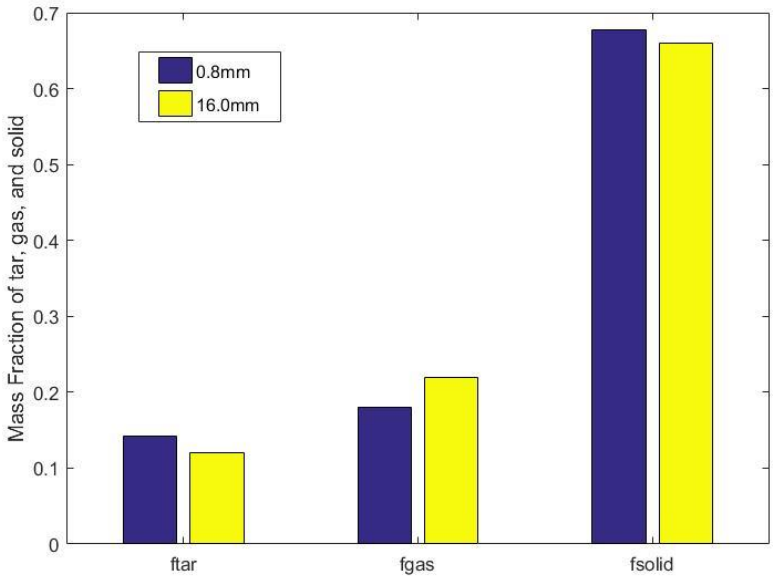

Figure 5-13. The comparison of the mass fraction of tar, gas and solid at the final time for 0.8mm and 16mm radius of coal particle at 785K

Next, we will examine the dependence of the chemical properties on the maximum imposed boundary temperature. The center of the particle is chosen for analysis. Fig. 5-14 shows the change of labile and charred bridge versus time at the center of the 0.8 mm radius of coal particle with the highest temperature of 785K and 873K.

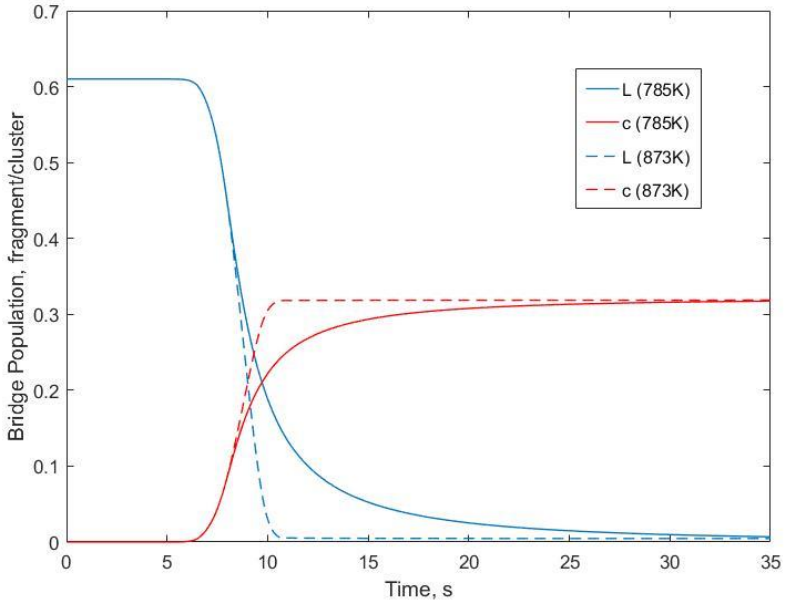

Figure 5-14. The change of labile and charred bridge versus time at the center of the 0.8mm radius of coal particle at 785K and 873K

Clearly pyrolysis proceeds faster as maximum temperature increases. Also, with the higher temperature, labile bridges can break and form charred bridge faster than lower temperature. Moreover, the pyrolysis of coal particle can be fully finished faster with the population of labile bridge goes to zero at the higher temperature.

Notably, even though the population of labile and charred bridges are almost identical at the end of pyrolysis due to the constant ratio of rates k_δ/k_c, Fig. 5-15 and 5-16 indicate that more tar and gas will be generated and released from the coal particle and finally the density of the coal particle decreases more as the maximum particle temperature increases. The reason is related to the size of fragments generated at different temperatures. After a labile bridge is cleaved, two halves of the side chains can stabilize to form fragments of large molecular weight. Tar is generated when a fragment has sufficiently low molecular weight to vaporize at a given temperature, as explained in Section B, Chapter

III. With increasing pyrolysis temperature, the mass of tar fragments becomes smaller, which is shown in Fig. 5-17, and they are more easily vaporized from the particle as tar. The mass of fragment depends on the expression of mass of fragments shown in Eq. 3.10. With the higher temperature, both the ratio of labile bridge and intact bridges *L/p*, and the total number of side chains δ_{total}, decrease and lead to the decreasing of the mass of tar fragment, which is shown in Eq. 3.10. Moreover, the mass fraction of light gas will increase with the domination of the increasing of the summation of the light gas formed from side chains, g_{total} (Eq. 3.9), which is shown in Fig. 5-18 and finally leads to the decreasing of density due to the decreasing solid fraction. Another contribution to the increase of tar is that the phase equilibrium constant, *Ki*, increases with increasing temperature, which also causes more liquid phase species to vaporize and increase the yield of tar.

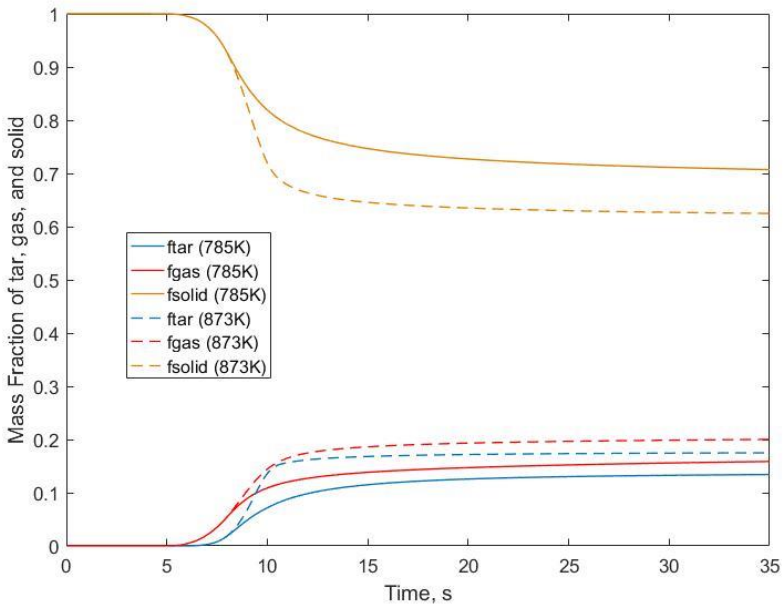

Figure 5-15. The change of mass fraction of tar, gas and solid versus time at the center of the 0.8mm radius of coal particle at 785K and 873K

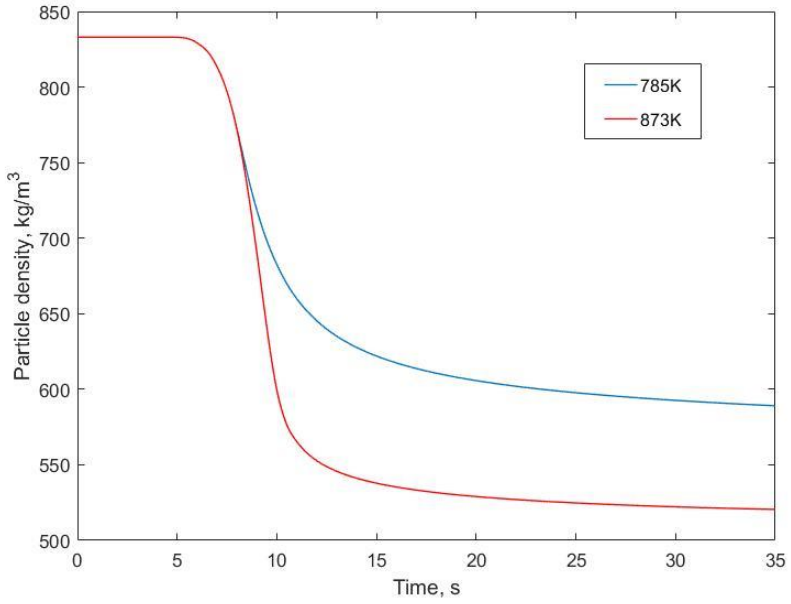

Figure 5-16. The change of density of particle versus time at the center of the 0.8mm radius of coal particle at 785K and 873K

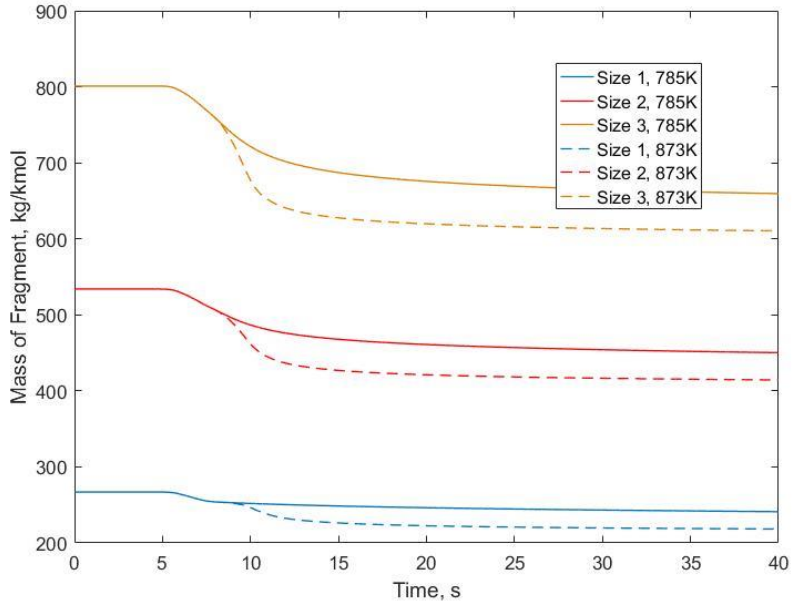

Figure 5-17. The size of fragments (less than 1000 kg/kmol) versus time at the center of the 0.8mm radius of coal particle at 785K and 873K

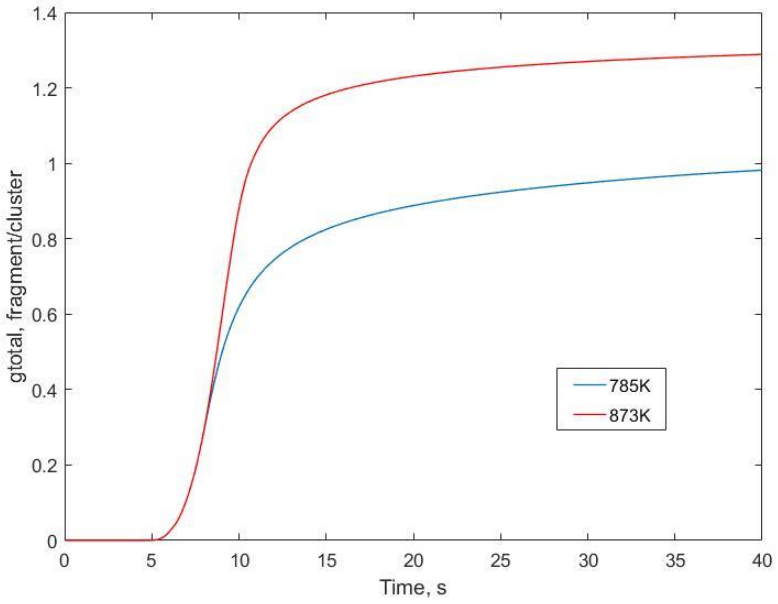

Figure 5-18. The change of g_{total} versus time at the center of the 0.8mm radius of coal particle at 785K and 873K

Figures 5-19 to 5-23 show the results for the 4.5 mm radius of the particles to support the discussion above. Pyrolysis takes longer with the larger particles, but similar to Figs. 5-14 and 5-16, irrespective of the maximum temperature, the final state of the bridges is the same. In other words, the maximum temperature determines the speed of the bridge breaking, but once pyrolysis starts, the labile bridge will break and eventually go to zero with the completion of pyrolysis. However, as in the discussion of Fig. 5-15 and 5-16, even though the labile bridges and charred bridges are same at the maximum temperature, the mass fraction of fragment depends on the maximum temperature, and then influence on the formation and the vaporization of the tar and gas, and leads to the density change of the particle after pyrolysis, which is also demonstrated in Fig.5-20 and 5-21.

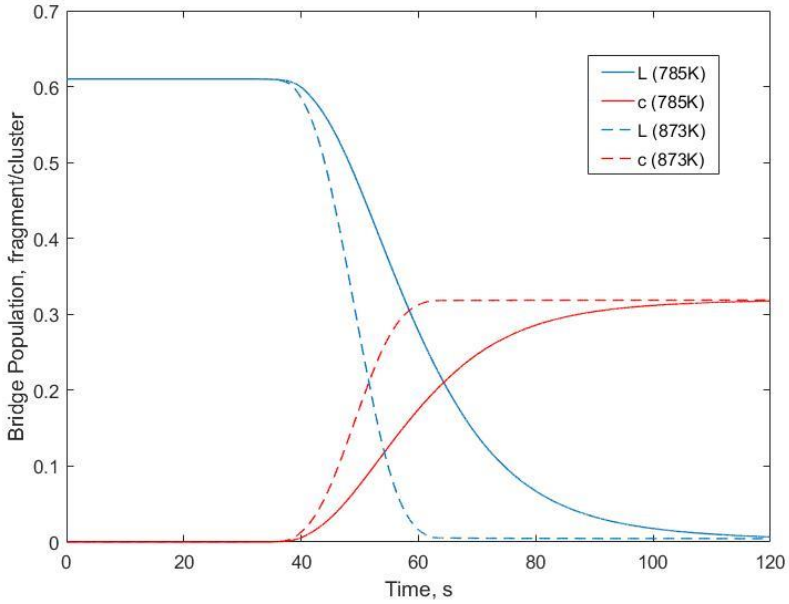

Figure 5-19. The change of labile and charred bridge versus time at the center of the 4.5mm radius of coal particle at 785K and 873K

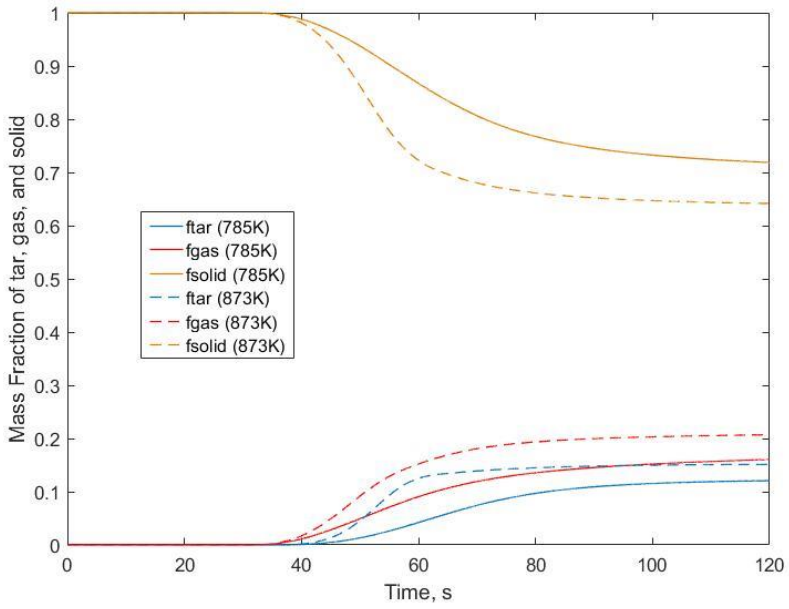

Figure 5-20. The change of mass fraction of tar, gas and solid versus time at the center of the 4.5mm radius of coal particle at 785K and 873K

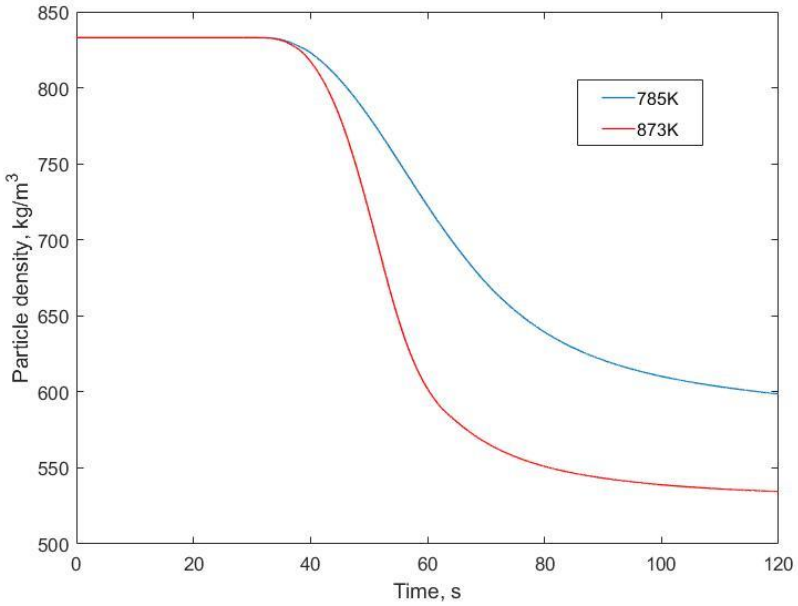

Figure 5-21. The change of density of particle versus time at the center of the 4.5mm radius of coal particle at 785K and 873K

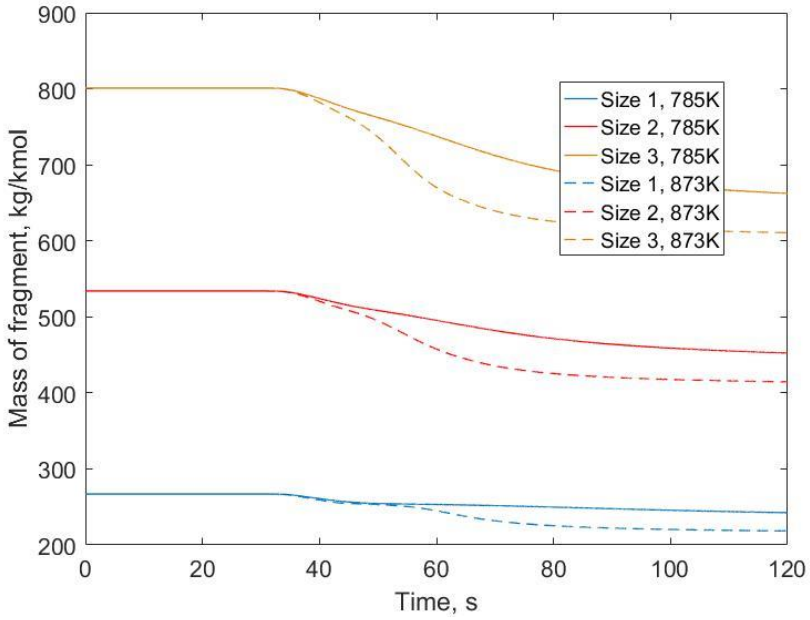

Figure 5-22. The size of fragments (less than 1000 kg/kmol) versus time at the center of the 4.5mm radius of coal particle at 785K and 873K

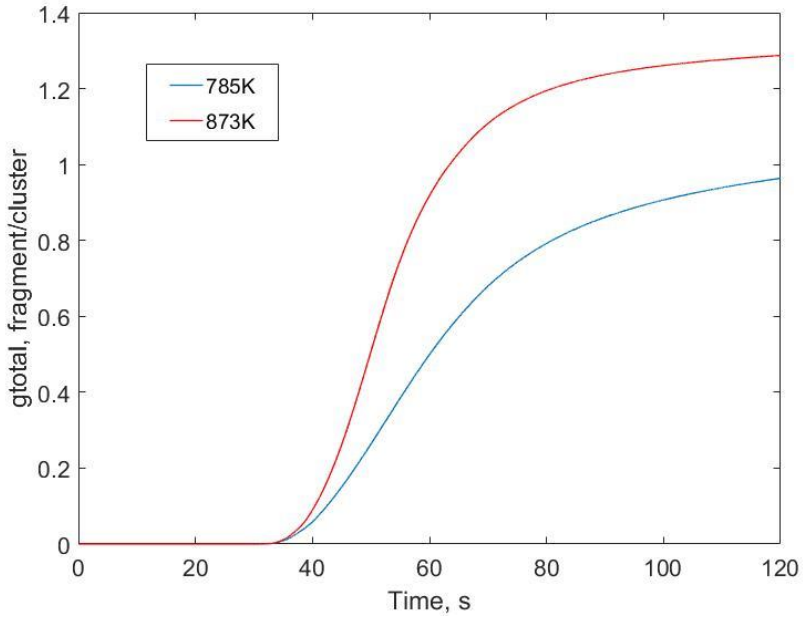

Figure 5-23. The change of g_{total} versus time at the center of the 0.8mm radius of coal particle at 785K and 873K

C. Model Validation

Before the improved CPD model can be used to study the generation of discrete tar species, the modeling capabilities shown in the last two sections will be compared with experimental data. Therefore, coal pyrolysis experiments that measured spatially-varying particle temperatures and overall pyrolysis yields will be used in this section to validate our particle-scale model. An experiment which has been performed by Zhang[27] with spatial resolution of particle temperature is used to compare with our model. In the experiment, Zhang and coworkers pyrolyzed 15 mm-radius spherical lignite particles at bulk gas temperatures of 713 K and 823 K, respectively. The residual mass fraction (m/m_0) and the particle center temperature, which have been obtained from the experiment, will be used to validate our model. Table 5-1 shows the CPD input parameters used to simulate the experiment of Zhang, which were chosen based on the similarity between the lignite used

by Zhang and the data of Zap lignite derived from NMR measurement.[27] Moreover, this validation just validate the modified CPD model and the heat transfer model, and does not validate the detailed discrete species model.

Table 5-1. CPD input parameters for the experiment of Zhang

p_0	c_0	$\sigma + 1$	MW_{cl}	MW_{δ}
0.63	0.1	5.23	308	46

Figure 5-24 and 5-25 compare simulation and experimental data for residual mass fraction and center temperature for pyrolysis of 10 mm and 15 mm radius particle at 713K.

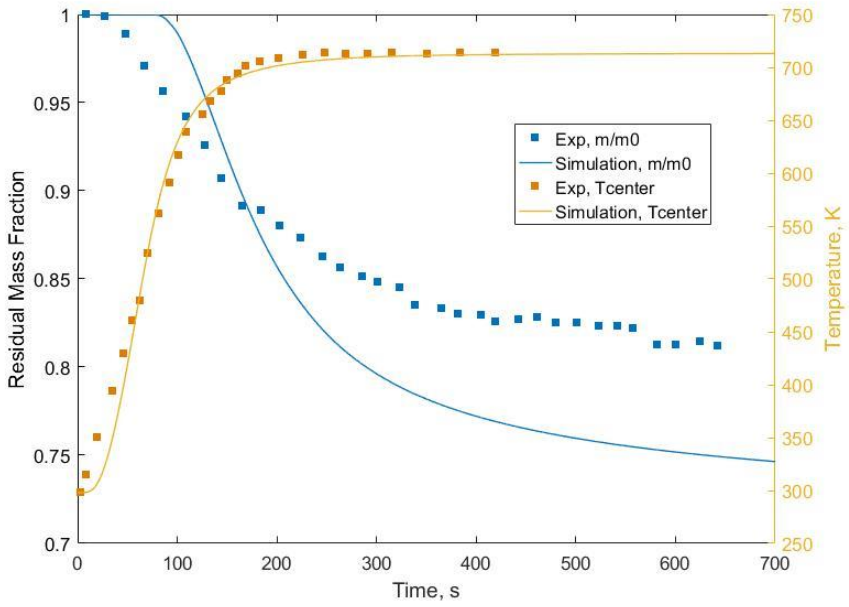

Figure 5-24. Simulation and experimental data for residual mass fraction and particle center temperature for pyrolysis of 10 mm radius particle at 713K

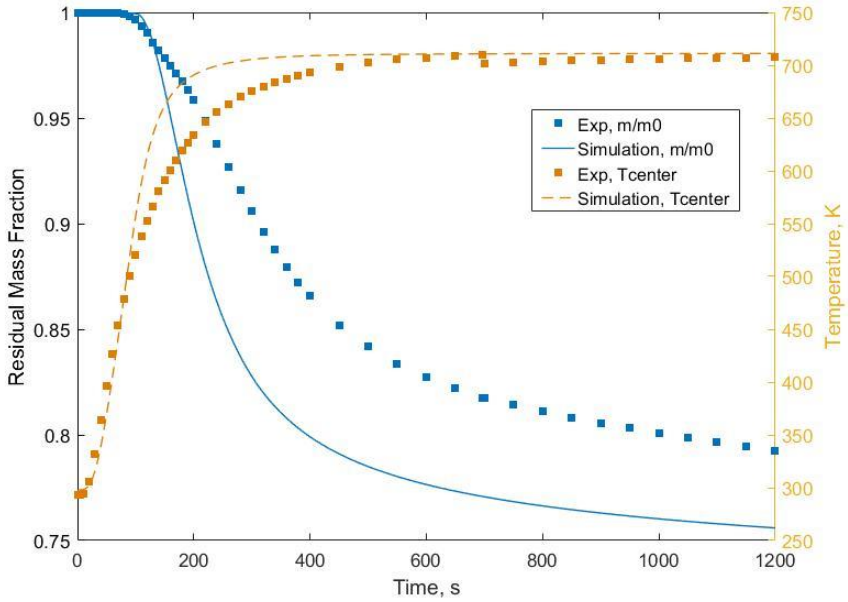

Figure 5-25. Simulation and experimental data for residual mass fraction and particle center temperature for pyrolysis of 15 mm radius particle at 713K

From the figures, although a deviation is observed, the center temperature of the particle has been predicted reasonably, especially given the uncertainty in the input parameters for coal particle, the actual chemical structure of the particle, and the exact heat transfer coefficient. On the other hand, the result of residual mass fraction does not exactly match due to the using of correlation instead of the coal-specific NMR-based parameters. This correlation is required for advanced pyrolysis model which can predict the chemical structure parameters of coals measured by ^{13}C NMR.[30] So, it is reasonable that the result from simulation can predict experimental data. Therefore, the ability of the model has been proved and it can be used for future pyrolysis research.

D. Tar and Discrete Species Generation

As the Chapter III mentioned, $\dot{V}$ is the vapor flow rate out of the particle, which describes the rate of tar and gas released from the particle, normalized by cluster, with units of *mol/(cluster·s)*. Based on Eq. 3.35 and Eq. 3.36, $\dot{V}$ may be different for different positions inside of the particle because the temperature gradient, which has influence on the variable K_i. Fig. 5-26 show the generation of $\dot{V}$ inside of the 0.8 mm radius particle at 785K for 1atm pressure condition.

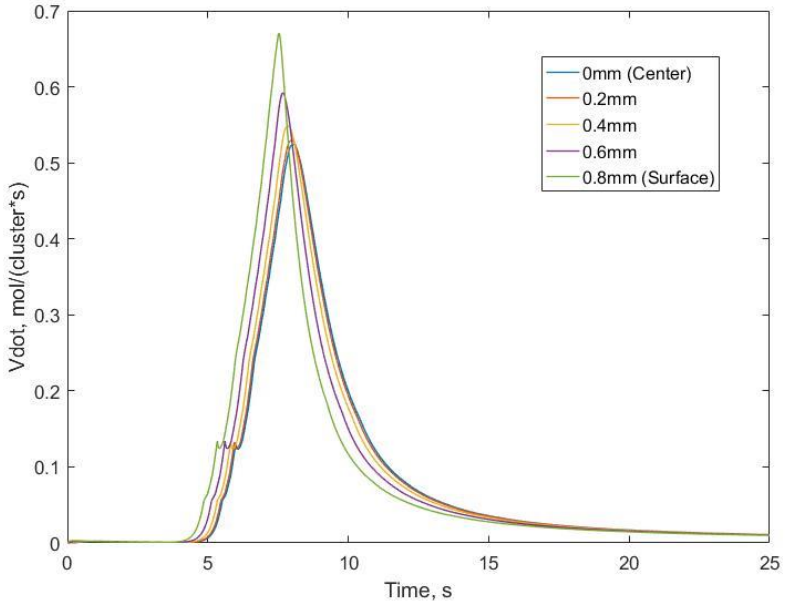

Figure 5-26. The change of $\dot{V}$ versus time inside of 0.8mm radius particle at 785K for 1atm pressure condition.

Fig. 5-26 indicates that the generation of vapor species begins from the surface of the particle, and with increasing temperature, more vapor species are generated by pyrolysis and exit the particle. However, $\dot{V}$ does not increase continuously with temperature during pyrolysis. $\dot{V}$ for every position has a maximum, which means it will

decrease after that time, due to the less generation of low molecular weight species that can vaporize from the liquid phase and exit the particle. Moreover, it does not increase continuously because no more bridges are breaking.

The impact of pressure on $\dot{V}$ can be examined using different pressure environments outside the particle. Fig. 5-27 shows the dependence of $\dot{V}$ on pressure at the center of the 0.8 mm radius particle at 785K for 1 atm, 2 atm and 5 atm pressure conditions.

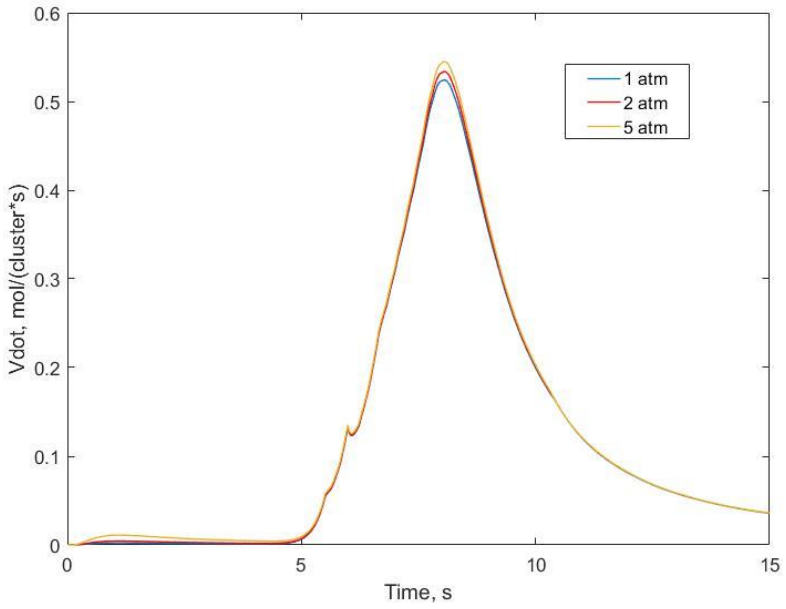

Figure 5-27. Comparison of $\dot{V}$ at the center of 0.8 mm radius particle at 785K for 1atm, 2atm and 5atm pressure condition

The result shows that the different pressure condition has a limited influence on the $\dot{V}$. The evolution of $\dot{V}$ during the process of pyrolysis is almost same. Pressure is not an important factor which can deeply influence the vapor flow rate of species out of the particle, even though increasing pressure can increase a little $\dot{V}$. The reason is that $\dot{V}$ is dominated by light gas, which depend on pressure. It is related to side chains and the

bridges which depends on the chemical structure. Therefore, it is possible that the $\dot{V}$ does not change too much with the change of phase equilibrium constant K_i.

We will now analyze results for the entire particle by integrating with respect to radius, either as a function of time or for complete pyrolysis, by also integrating the results in time. These spatially-integrated results are more industrially-relevant, given that the quantity of interest is often the flux of species or total production of species from the particle as a whole. Many pyrolysis processes run to completion and the quantity of interest in this case is the final yields of gas, tar species and char, obtained from integrating with respect to radius and time.

First, $\dot{V}_{total}$ for the whole particle can be obtained by using a conversion factor, AB, with units of *cluster/m*^{3}, to convert $\dot{V}$ from *mol/(cluster·s)* to *mol/m*^{3}*·s and* integrating over the particle volume:

$$AB = 1000 \times \frac{Density\ of\ Particle}{m_{total}} \tag{5.1}$$

$$\dot{V}_{total} = 4 \cdot AB \cdot \pi \cdot \int_0^R r^2 \dot{V}\,(r) dr \tag{5.2}$$

where m_{total} is the total molar mass per cluster, which is shown in Eq. 3.11. In this way, Fig. 5-28, which shows the total vapor flow rate of species out of the particle for the whole 0.8 mm radius particle versus time, can be obtained.

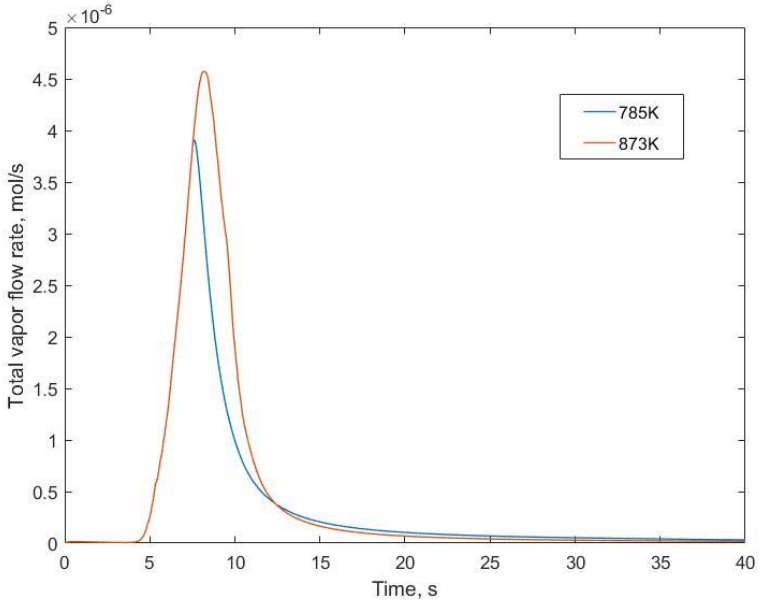

Figure 5-28. Total vapor flow rate of species out of the particle for the whole 0.8mm radius particle versus time at 785K and 873K

From this figure, it is seen that the total vapor flow rate of species out of the particle (for the whole particle) is a function of temperature. Before 7.5 s, the temperature is the same for both of two imposed temperature boundary conditions and $\dot{V}$ for whole particle is same. Based on Fig. 5-1, the temperature does not increase continuously after 7.5s for the 785 K case and $\dot{V}$ for whole particle begins to decrease, which is shown as the blue line in Fig. 5-28. However, for the 873 K case, the temperature continues to increase beyond 7.5s and makes $\dot{V}$ for whole particle release more than the lower temperature (red line). And it also decreases after the temperature reaches the maximum, 873K. Both of them will go to near zero finally, which indicates the pyrolysis is almost finished. Moreover, if we integrate $\dot{V}$ over radius and temperature together, we can get the total vapor of all species out of the particle for the 0.8 mm radius particle during the entire process of pyrolysis.

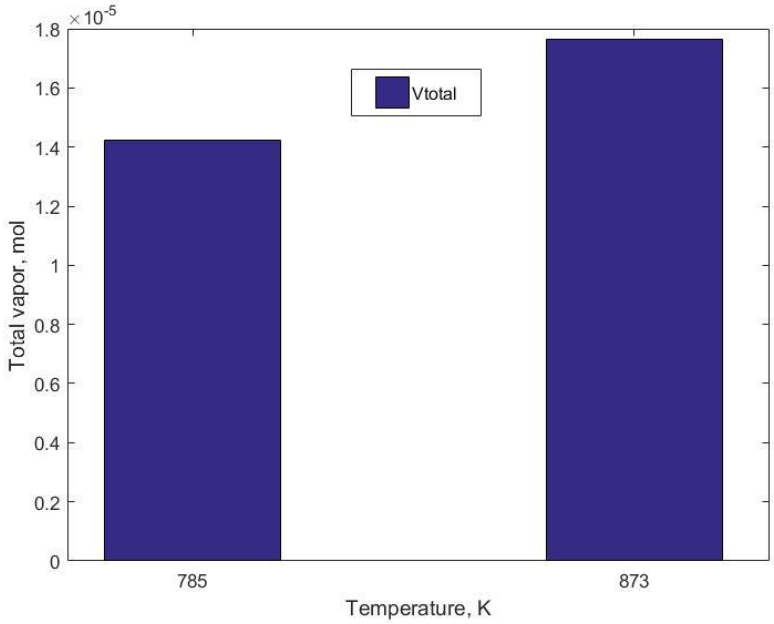

Figure 5-29. Total vapor of species out of the particle for the whole 0.8mm radius particle versus time at 785K and 873K

In terms of whole particle scale during the entire pyrolysis, the total vapor flow for all species out of the particle is higher with the higher temperature, which is shown in Fig. 5-29. The reason for that has been discussed that higher temperature can make the fragments smaller and more small molecular species can be vaporized, and the increasing percentage of total vapor flow is approximately proportional to the sum of increasing percentage of tar and gas fraction in Fig. 5-15, which is 27%.

The full discrete species model can be used to obtain the generation of every particular species at every single time or the total vapor released for every particular species. The original CPD model cannot predict the detailed tar species, which are very important when pyrolysis is used to produce chemicals. Our improved CPD model is simple that a simple way of dividing the number fraction of fragments into particular species is used. Nevertheless, we developed the capability to model discrete species with computational

efficiency. In what follows, $\dot{V}_i$ for particular tar species are shown, based on the multiplication of $\dot{V}$ and the mole fraction of the species in the vapor phase.

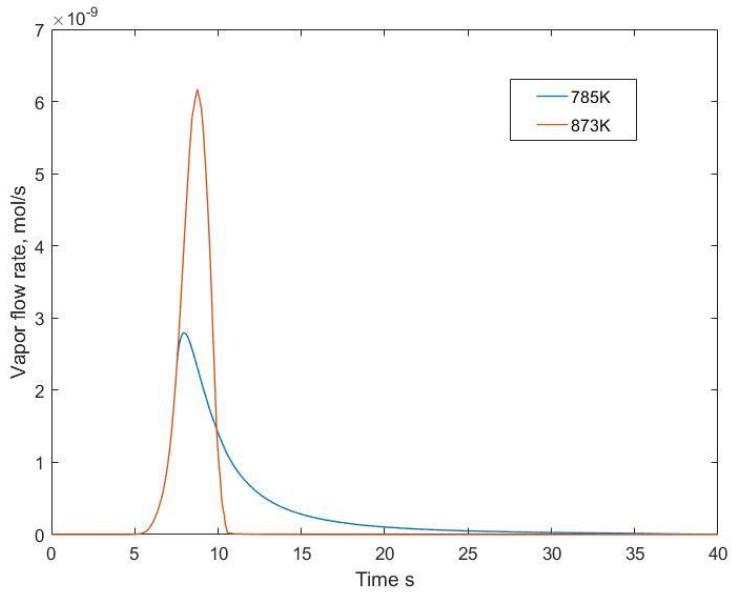

Figure 5-30. Vapor flow rate of species (Molecular Weight 150 kg/kmol) out of the particle for the whole 0.8mm radius particle versus different times at 785K and 873K

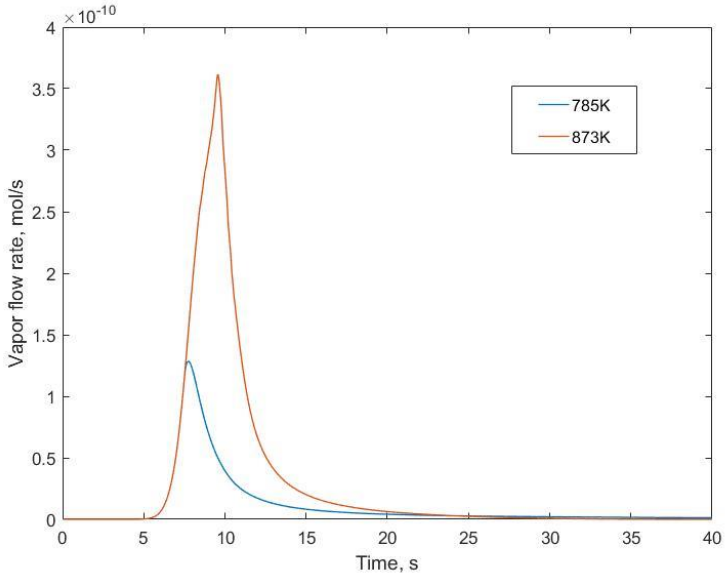

Figure 5-31. Vapor flow rate of species (Molecular Weight 542 kg/kmol) out of the particle for the whole 0.8 mm radius particle versus different times at 785K and 873K

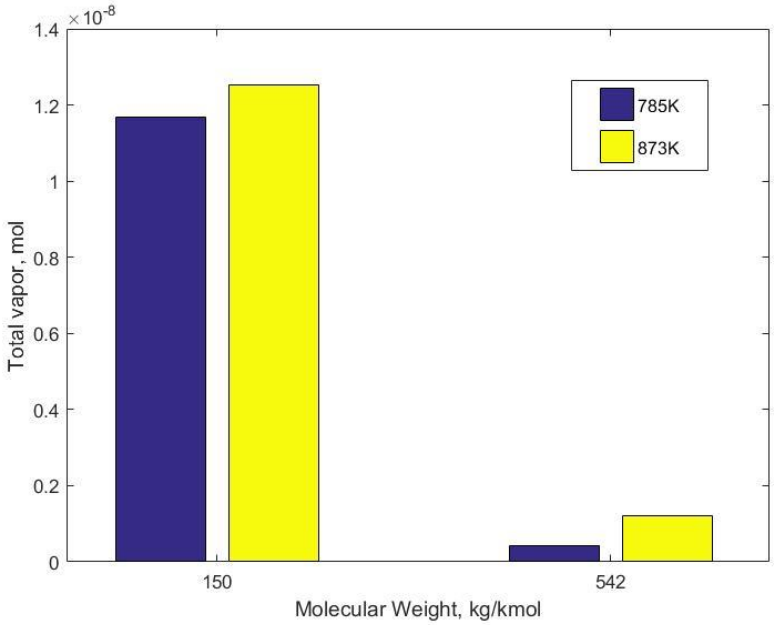

Figure 5-32. Total Vapor of two particular species out of the particle for the whole 0.8mm radius particle at 785K and 873K

Also, the total vapor of these two particular species out of the particle for the 0.8 mm radius particle during the entire process of pyrolysis can be obtained by integrating over time as well, as shown in Fig. 5-32. It is clear that higher temperatures increase the release of tar species from the particle in general. The reason for that is related to the generation of fragments, which has been shown in Fig. 5-18. What is more, the vapor flow rate for small molecular weight is higher than large molecular weight. It indicates that small molecular weight species Also, the results for the same species can be got from larger particles, and the comparison of more individual tar species can be seen in Fig. 5-35.

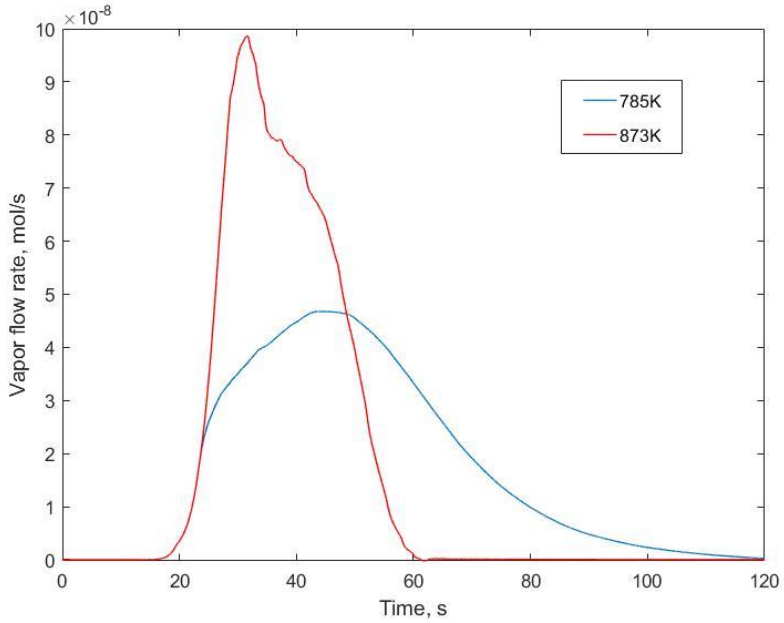

Figure 5-33. Vapor flow rate of species (Molecular Weight 150 kg/kmol) out of the particle for the whole 4.5 radius particle versus different times at 785K and 873K

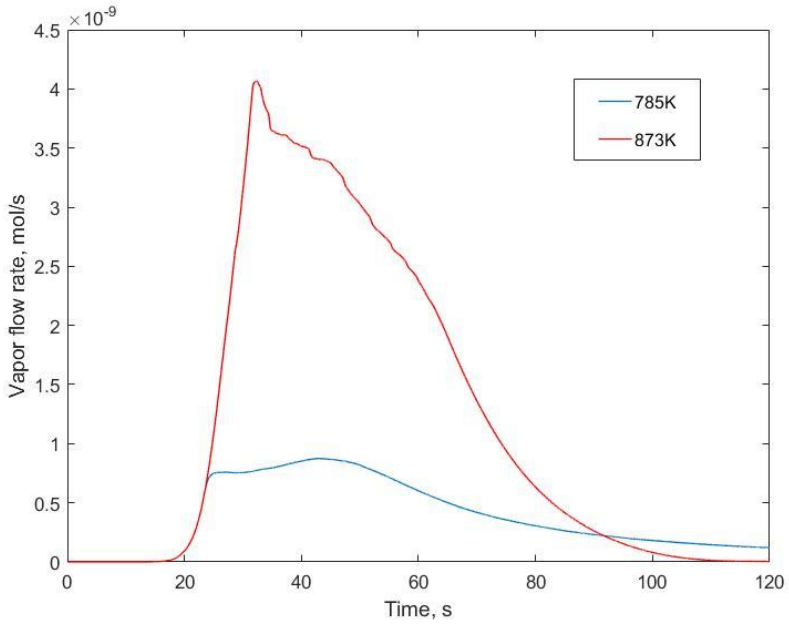

Figure 5-34. Vapor flow rate of species (Molecular Weight 542 kg/kmol) out of the particle for the whole 4.5 radius particle versus different times at 785K and 873K

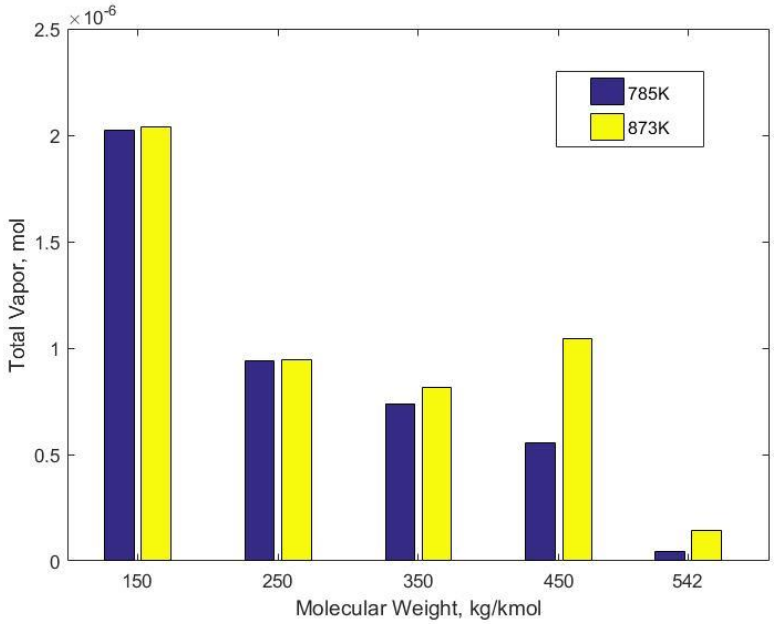

Figure 5-35. Total Vapor of several particular species out of the particle for the whole 4.5mm radius particle at 785K and 873K

Figures 5-33 and 5-34 shows the vapor flow rate of the same species for a larger particle situation. Again, higher temperature accelerates the vapor flow rate, which has been just discussed. What is more, from Fig. 5-35, higher temperature can release more species out of the particle than lower temperature, especially large molecular weight species. The reason for this fact is related to the increasing of *Ki* with the increasing of temperature, which can transfer more liquid phase species into vapor phase and vaporize out of the particle. In terms of small molecular weight species, the value of *Ki* is much larger than one for both temperature conditions, which leads to a smaller difference between the two cases, which can be seen in Fig. 5-35.

Next, Figure 5-36 shows the total vapor of particular species out of the 0.8 mm radius particle at 785K for different pressure.

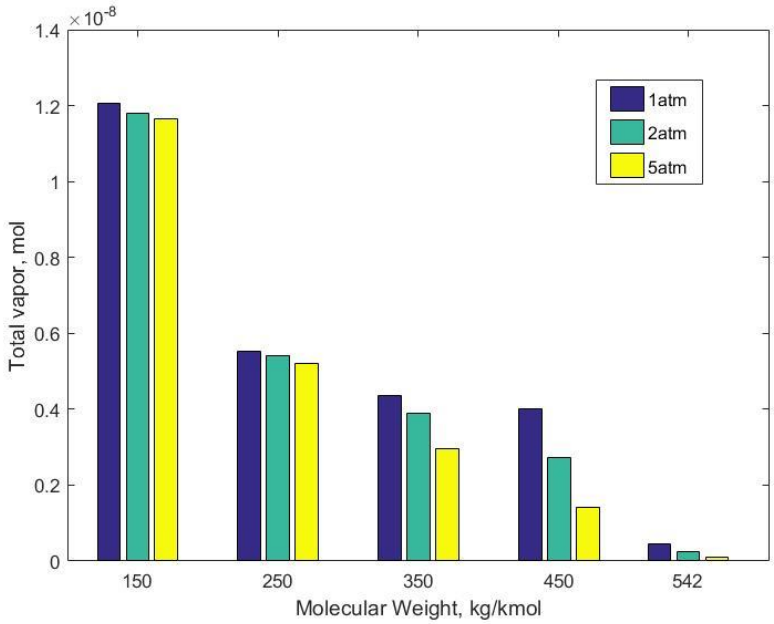

Figure 5-36. Total vapor of particular species out of 0.8 mm radius particle at 785K for 1atm, 2atm and 5atm pressure condition

Figure 5-36 proves that the total vapor for tar species is related to the pressure. The higher the pressure is, the less the tar species vaporize out of the particle. Moreover, it can prove that the similar $\dot{V}$ under different pressure conditions, which is shown in Fig. 5-27, is not dominated by tar species. Therefore, another part of the gas volatiles, light gas, which is not related to the pressure, determines the $\dot{V}$.

Figure 5-37 shows the comparison of total production of several species per volume which are different molecular weight at the final time for 0.8mm and 16mm radius of coal particle at 785K. And the error percentage between the two sizes of particles are shown in the figure. It is clear that the smaller size of particle products much more species per volume than larger size of particle, and the error becomes larger and larger with the increasing of molecular weight of species. Therefore, this is another reason for resolving

spatially the particle if we really want to know the accurate generation for particular species for different size of the particles.

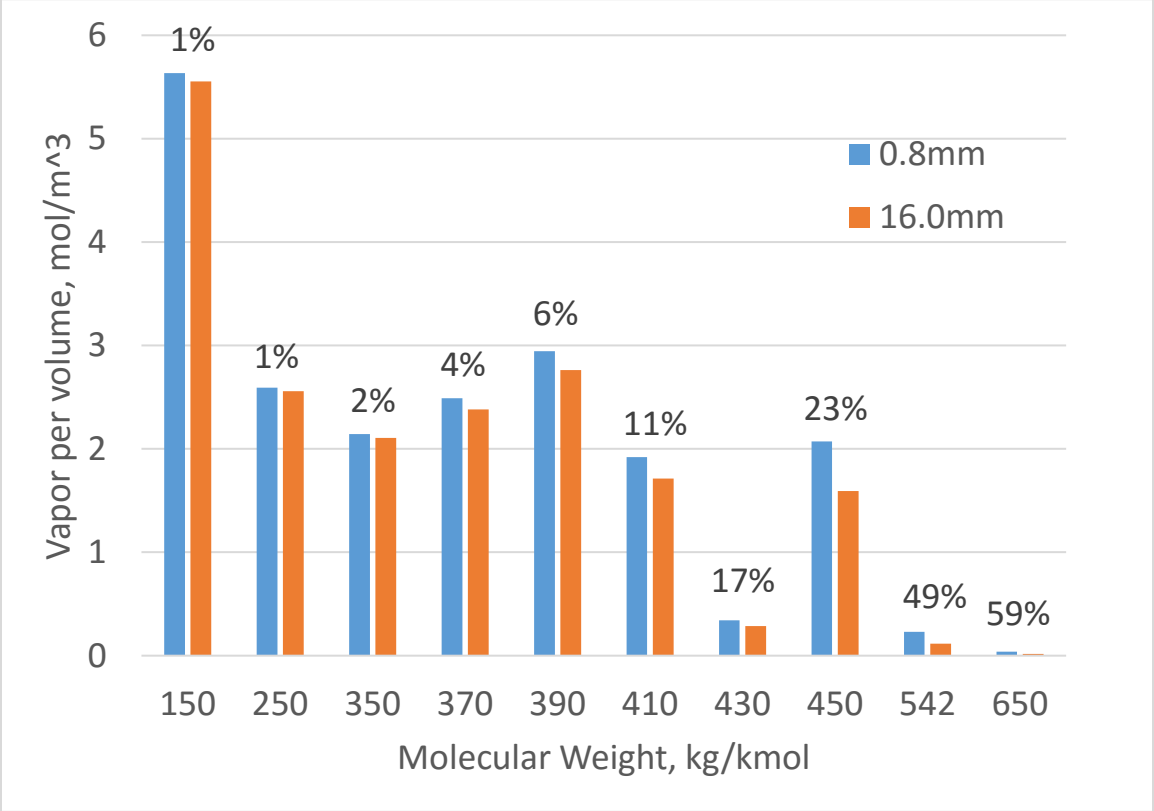

Figure 5-37. The comparison of total production of particular molecular weight per volume at the final time for 0.8mm and 16mm radius of coal particle at 785K

Finally, the comparison between the full discrete species model and DQMoM + Delumping model will be analyzed. Our ultimate goal is using the DQMoM + Delumping model instead of full discrete species model to save the computational time. Therefore, the results of key variables, such as $\dot{V}$, from the two models should be approximately same.

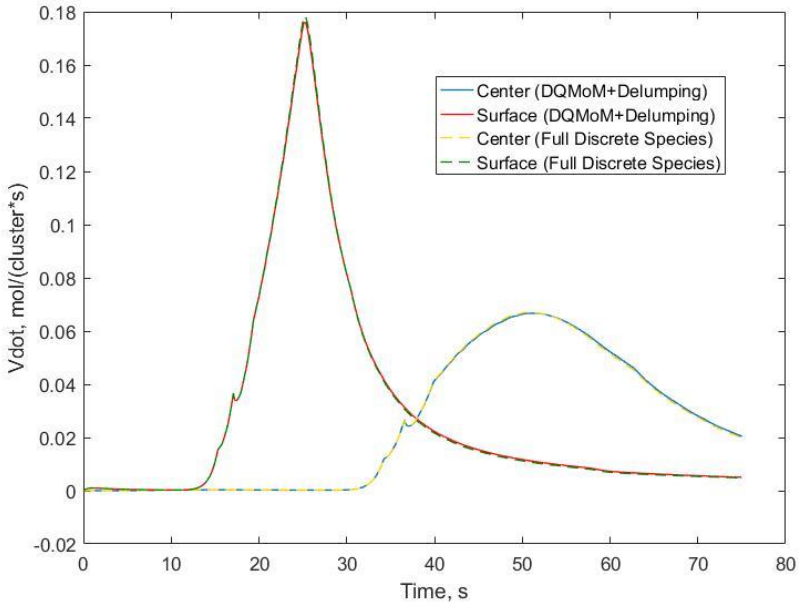

Figure 5-38. Comparison of $\dot{V}$ at the center and surface of 4.5mm radius particle for two models.

It is clear from Fig. 5-38 that although $\dot{V}$ in full discrete species model is calculated through the exact discrete species (Eq. 3.31), while in DQMoM + Delumping model is calculated through the weight and nodes, the result from the two models are almost exactly same at different positions inside of the particle.

After finishing the discussion of discrete species generation of the improved CPD model, next two figures will show the result of DQMoM model. As the Chapter IV mentioned, DQMoM model uses the weights and nodes instead of the mole fraction and the molecular weight of fragment. Figs. 5-39 and 5-40 shows the evolution of the weight and node for 0.8mm radius particle. Both of them are well-behaved. Also, it is clear that node 1 represents the lump species which has the smallest molecular weight, and the weight of node 1 decreases in Fig. 5-39. It means the small molecular weight species vaporizes out of the particle, which matches the result shown above.

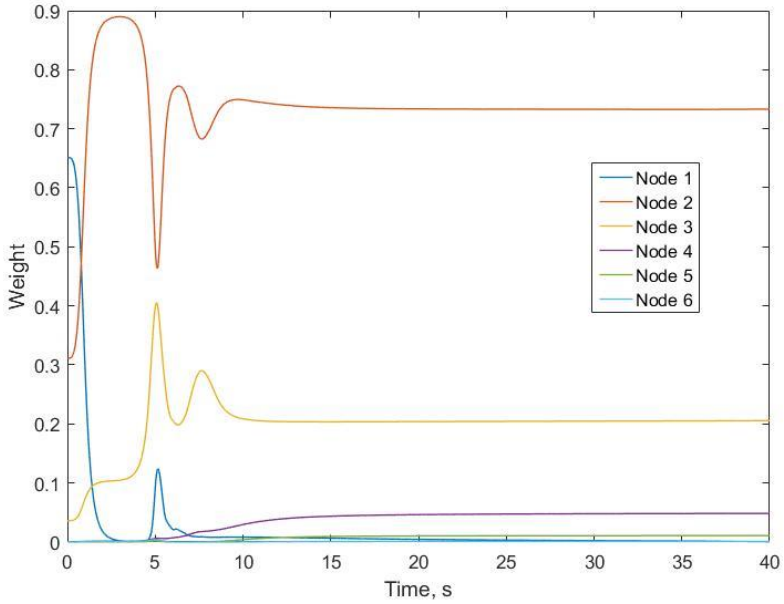

Figure 5-39. Evolution of weight at the center of 0.8mm radius particle for DQMoM model.

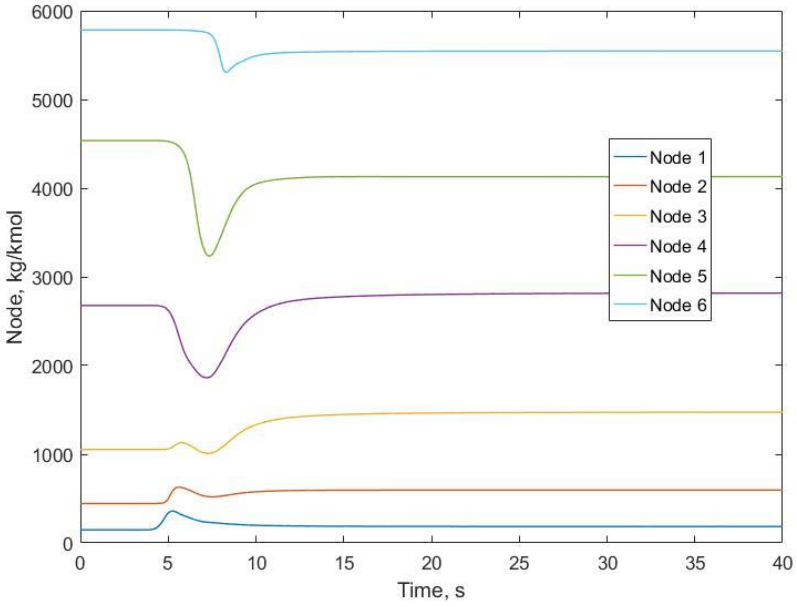

Figure 5-40. Evolution of node at the center of 0.8mm radius particle for DQMoM model.

Furthermore, we can compare the individual species mole fractions calculated by the two models separately. Recall, the full discrete species model solves the ODEs of every species directly, while the DQMoM + Delumping model gets results for every species through "delumping" the results of the calculation with only a few weights and nodes.

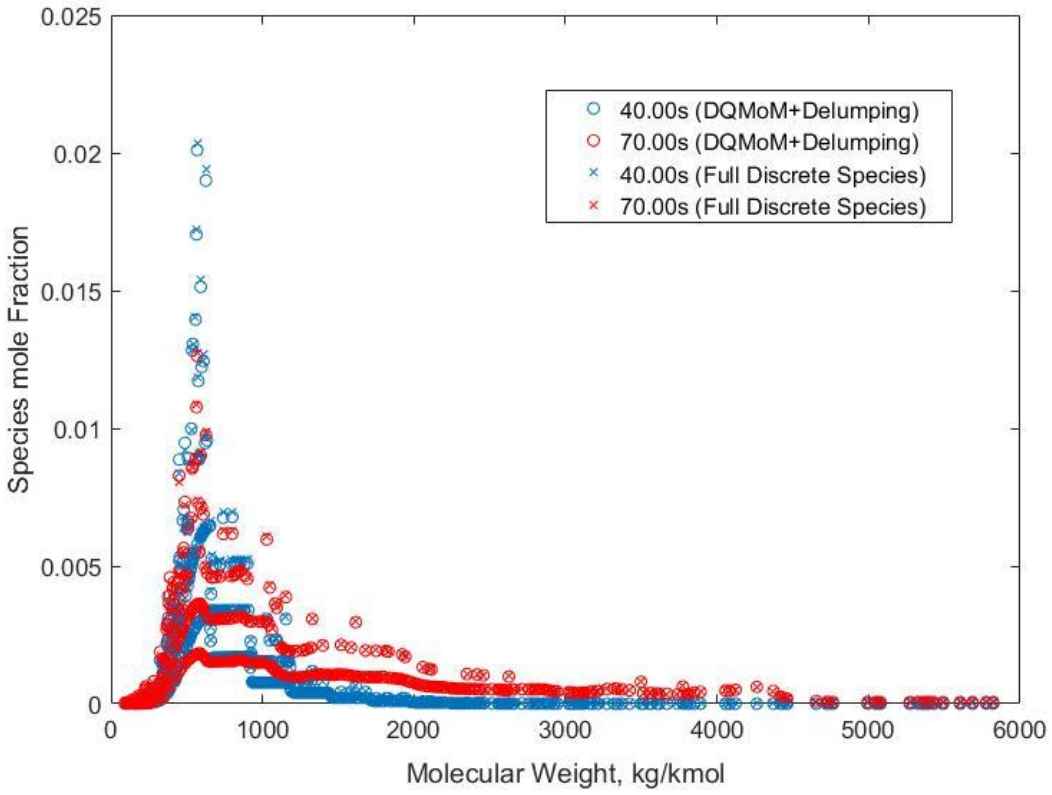

Figure 5-41. Comparison of species Distribution at the center of 4.5mm radius particle at 785K for two models at different times.

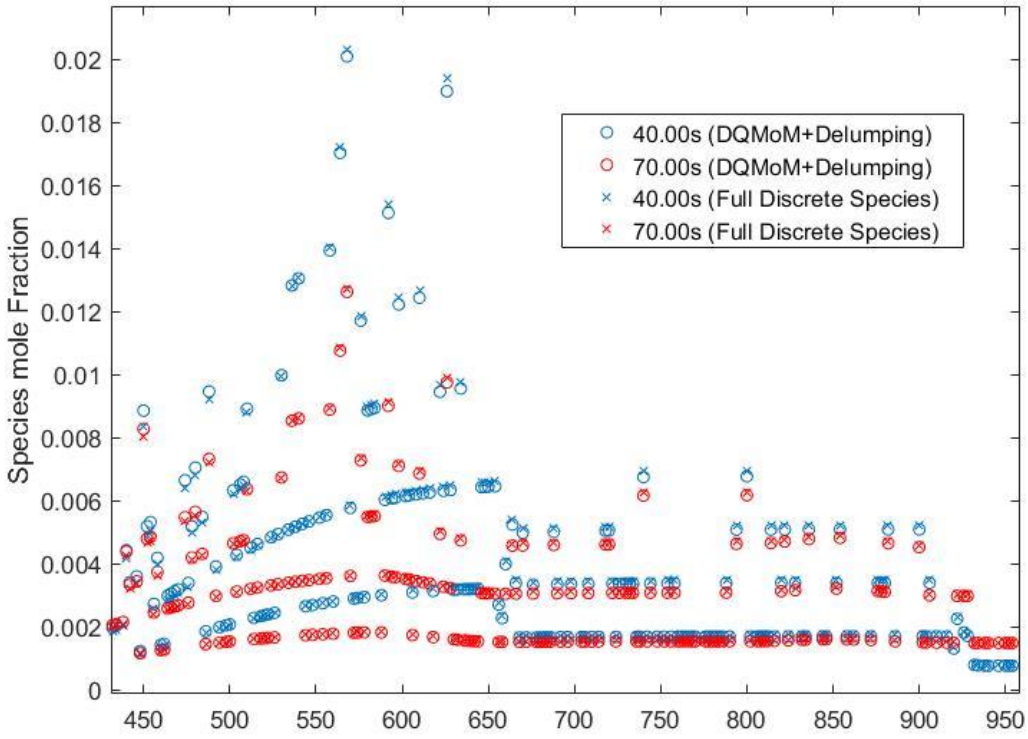

Figure 5-42. Comparison of species Distribution (Molecular Weight 450-950 kg/kmol) at the center of 4.5mm radius particle at 785K for two models at different times.

Figures 5-41 and 5-42 compare the result of species distribution between the full discrete species model and DQMoM + Delumping model. Fig. 5-42 is a "zoomed in" figure from Fig. 5-41 for the molecular weight from 450 to 950 kg/kmol. First we compare the discrete liquid species distribution within the metaplast at every time step from the full discrete species model and DQMoM + Delumping model. Moreover, Fig. 5-41 and 5-42 select two time steps: 40 seconds, when the pyrolysis just starts and 70 seconds, when the pyrolysis almost finishes. It can be seen that the distribution of discrete species changes a lot during the process of pyrolysis. The species with large molecular weights has been generated during the period of pyrolysis, meanwhile the mole fraction of species with small

molecular weights decreases a lot because of the vaporization of the species with small molecular weight, which has been proved through Fig. 5-36.

The molar flux of every species, which is the product of $\dot{V}$ and the gas-phase mole fraction of that species, is more valuable to compare. In terms of detailed chemical kinetic mechanisms, the molar flux of each species is more important for simulations than the mole fraction of discrete liquid species distribution. Moreover, if the relative error for the flux of each species between two models is smaller than 10%, it is reasonable to use the DQMoM + Delumping model, which has computational efficiency. The next figures will show the discrete species flux for two models at different times and the relative error between two models.

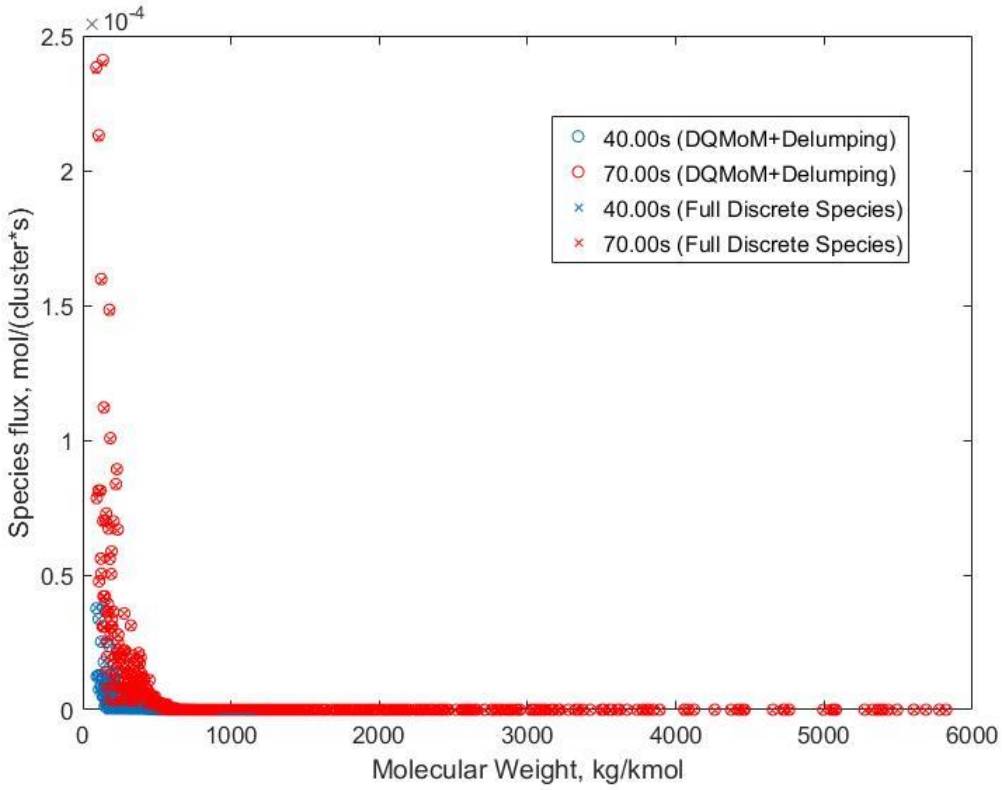

Figure 5-43. Comparison of species flux at the center of 4.5mm radius particle at 785K for two models at different times.

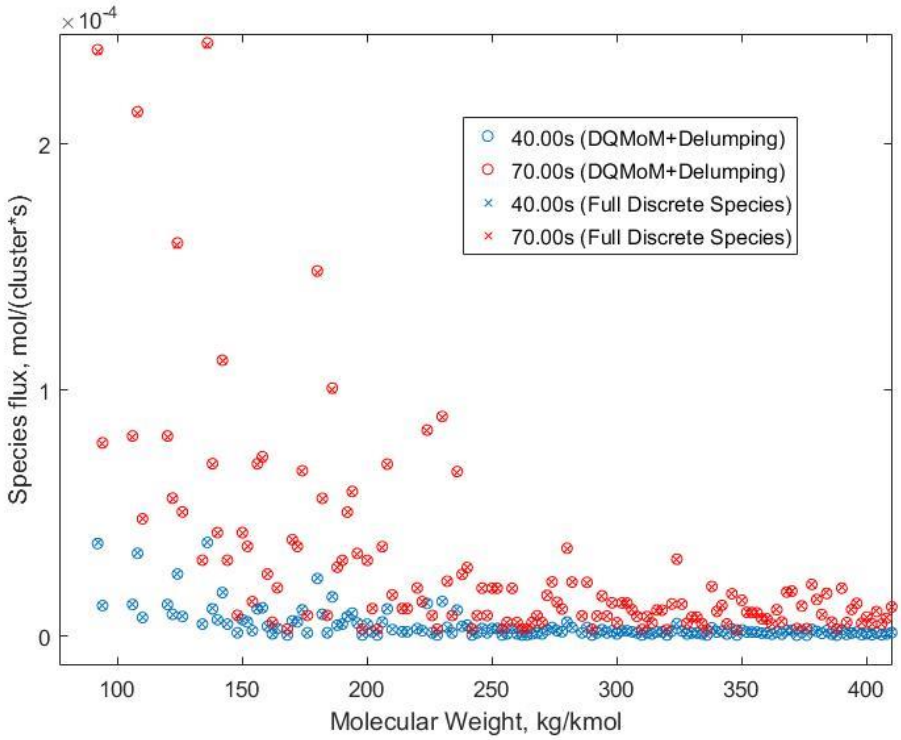

Figure 5-44. Comparison of species flux (Molecular Weight 92-400 kg/kmol) at the center of 4.5mm radius particle at 785K for two models at different times.

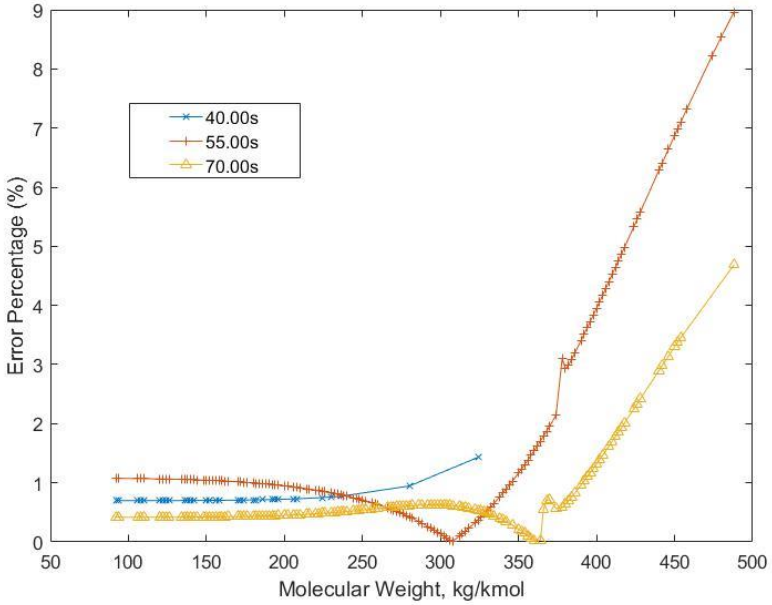

Figure 5-45. The relative error between the species flux of two models at the center of 4.5mm radius particle at 785K at different times.

Fig. 5-43 shows the comparison of species fluxes for the two models at the center of 4.5 mm radius particle at 785K, and Fig. 5-44 is a "zoomed in" figure from Fig. 5-43 for the molecular weight from 92 to 400 kg/kmol. The agreement is very good for all species and all time. Fig. 5-45 shows the relative error for species with absolute flow rates in excess of 0.5×10^{-5} *mol/s*, and entries which are small than that are neglected. It is clear that for all times, the relative error is smaller than 10%. That means the result obtained from two models are almost the same. The DQMoM + Delumping model can achieve the same accuracy as the full discrete species model by solving only twelve differential equations, meanwhile, more than 600 differential equations are solved by the full discrete species model.

Last, but not least, the computational time is also very important for both models. Fig. 5-46 shows the comparison of computational time for full discrete species model and DQMoM + Delumping model for different temperature.

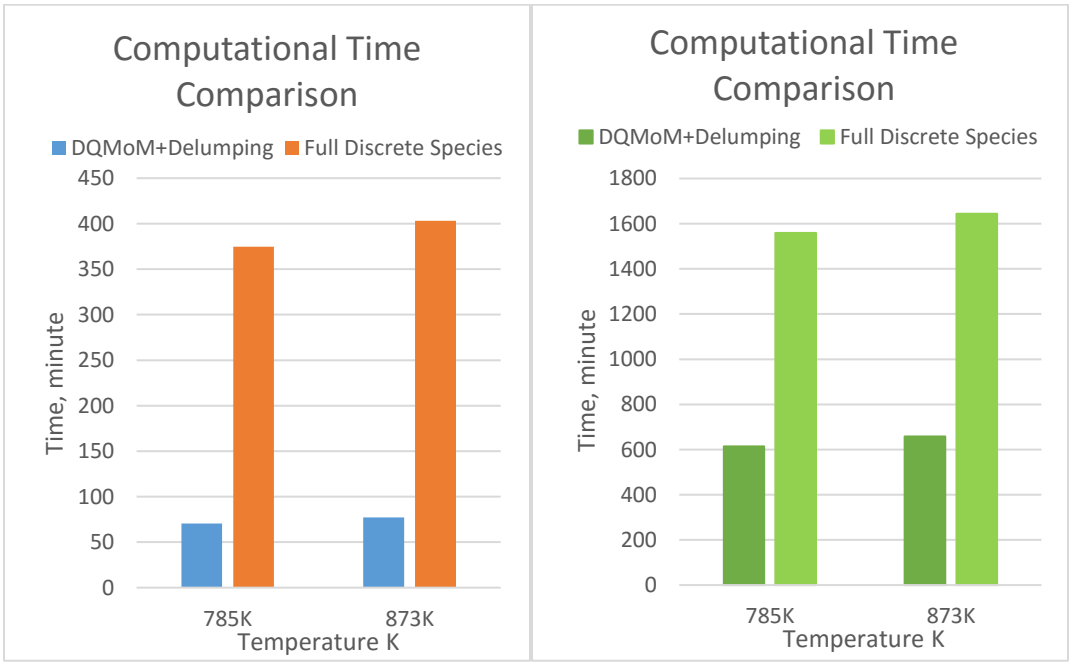

Figure 5-46. Comparison of Computational time for (1) 0.8mm radius particle for different temperatures. (2) 4.5mm radius for different temperatures.

The computational time of 0.8 mm radius particle for DQMoM + Delumping is approximately 70 minutes, and that for full discrete species model is nearly 375minitus. Moreover, for the larger particles, the computational time will be extended due to a longer time range and more grid points (and ODEs). So, the computational times of 4.5 mm radius particle for DQMoM + Delumping and full discrete species model are nearly 10 hours and 30 hours. Therefore, from Fig. 5-41 to 5-44, the results from different models can almost exactly match each other, and the relative error is smaller than 10%, which means the DQMoM + Delumping model can replace the full discrete species model to predict the discrete species distribution at every single time with saving almost 80% computational time for the 0.8 mm radius particle and 60% for 4.5 mm radius particle. The reason for the lower computational efficiency of larger particles is that larger particle uses more grid points, which means the computational overhead associated with solving the differential–algebraic system will be larger. During the calculation process, the computational speed will decrease when the pyrolysis starts. However, with the larger particles, the initial time for pyrolysis at different grid points is different due to the temperature gradient. Even though the pyrolysis finishes at the surface of the particle, the computational speed will not increase because the pyrolysis is still going inside of the particle. Therefore, the computational efficiency is low from the initial time of pyrolysis at the surface and to final time of pyrolysis at the center.

Chapter VI Conclusion & Future Work

A. Conclusion

A full discrete species model with improved VLE method for full discrete species has been developed in this paper. This model can be used to simulate the process of pyrolysis and get the detailed discrete species generated. Also, the improved VLE method is a continuous method which employs the rate-based flash calculations. Compared with the previous CPD model, the improved model can calculate not only the change of chemical structure based on fragments and clusters, but also the change of individual discrete species during pyrolysis. And it also can predict the behavior of pyrolysis and the release of vapor species for the particle scale. What is more, the previous CPD model uses the VLE model based on a discontinuous mole-based flash calculation, and it has disadvantage on time-step dependence. However, the improved VLE method can eliminate the negative influence on time-step dependence, which has highly influence on the fraction of total vapor (*V/F*), and get more accurate result with transient time.

In this study, the full discrete species model is applied to large-scale particle, which the temperature influence inside of it is not negligible due to the size of the particle. Therefore, the thermal energy conservation equation has been used in this study to model the change of temperature during the pyrolysis, and the finite volume method is applied to discretize the terms in the equation and obtain the temperature profile at different positions inside of the particle. More importantly, the development of finite volume method on the thermal energy conservation equation develops the CPD model from researching one single

position to multiple positions, which is very useful to simulate the pyrolysis of large-scale coal particle.

Another improvement in this paper is using the DQMoM model to simulate the pyrolysis based on CPD model and then delump the result to get the full discrete species generated at every time step. DQMoM method is an effective numerical way to solve the problem about the continuous thermodynamics. Compared with the CPD model, which is developed in terms of fragments, DQMoM is developed with the evolution of the nodes and weights in equivalent liquid-phase mole fraction distribution. Also, the result of DQMoM is based on the "lumped" species which are amounts of species with similar molecular weight. Therefore, the delumping method with the using of integrate factor has been developed to solve the species equation in terms of every discrete species. In this study, the DQMoM + Delumping model is applied to get the distribution of more than 500 discrete species and the results are almost exactly same with the results solved by full discrete species model. And the computational time for DQMoM + Delumping model is three times less than the full discrete species model. The DQMoM + Delumping model has a big advantage in computation time while providing the same results of discrete species with excellent accuracy.

B. Future Work

Right now, the number fraction of all discrete species generated at every time step (from the original coal structure, prior to vapor-liquid equilibrium) is determined by the number fraction of all discrete species at final time obtained from a detailed chemical simulation by collaborators at MIT. Thus, this paper employs a simple relationship between the number fraction of all discrete species generated at every time step and the final time,

and the reality is surely more complicated. Therefore, future work will focus on deriving an improved equation based on Eq. 3.18 to describe the more accurate number fraction of all discrete species at every time. The current method serves as a placeholder and is used to demonstrate the other model developments outlined above.

Even though DQMoM + Delumping has a significant advantage in computational efficiency compared to the full discrete model, the computational time is still too long to simulate larger scale particle with more grid points inside of the particle. The reason is that at the beginning of the pyrolysis, it costs much time to calculate the $\dot{V}$, which is determined by the algebraic equation in the DAE system. And the beginning of the pyrolysis at different positions inside of the particle is different. That means the process of calculation does not become fast until the beginning of the pyrolysis finishes for all positions. In the future, the method of integrating the system equations will be optimized to reduce computational time.

BIBLIOGRAPHY

[1] Adesanya, Babafemi A., and Hoanh N. Pham. "Mathematical modelling of devolatilization of large coal particles in a convective environment." *Fuel* 74.6 (1995): 896-902.

[2] Bruyat, A., C. Laurent, and O. Rouzaud. "Direct quadrature method of moments for multicomponent droplet spray vaporization." *International Conference on Multiphase Flow*. 2010.

[3] Baum, M. M., and P. J. Street. "Predicting the combustion behaviour of coal particles." Combustion science and technology 3.5 (1971): 231-243.

[4] Cotterman, Ronald L., and John M. Prausnitz. "Flash calculations for continuous or semicontinuous mixtures by use of an equation of state."*Industrial & Engineering Chemistry Process Design and Development* 24.2 (1985): 434-443.

[5] Fletcher, Thomas H., et al. "A chemical percolation model for devolatilization: summary." *Brigham Young University* (1992).

[6] Kobayashi, Howard, J. B. Howard, and Adel F. Sarofim. "Coal devolatilization at high temperatures." Symposium (international) on combustion. Vol. 16. No. 1. Elsevier, 1977.

[7] Gupta, Parthapratim, and Ranjit Kumar Saha. "Analysis of gas–solid noncatalytic reactions in porous particles: finite volume method." *International journal of chemical kinetics* 36.1 (2004): 1-11.

[8] Niksa, Stephen. "Rapid coal devolatilization as an equilibrium flash distillation." AIChE journal 34.5 (1988): 790-802.

[9] Jatoba, L. F. C., et al. "Simulation of the compressible flow with mass transfer of semi-continuous mixtures using the direct quadrature method of moments." *Computers & Chemical Engineering* 64 (2014): 153-166.

[10] Jupudi, Ravichandra S., Vladimir Zamansky, and Thomas H. Fletcher. "Prediction of light gas composition in coal devolatilization." *Energy & Fuels* 23.6 (2009): 3063-3067.

[11] Lage, Paulo LC. "The quadrature method of moments for continuous thermodynamics." *Computers & chemical engineering* 31.7 (2007): 782-799.

[12] Laurent, Claire, Gerard Lavergne, and Philippe Villedieu. "Quadrature method of moments for modeling multi-component spray vaporization." *International Journal of Multiphase Flow* 36.1 (2010): 51-59.

[13] Laurent, Claire, Gerard Lavergne, and Philippe Villedieu. "Continuous thermodynamics for droplet vaporization: Comparison between Gamma-PDF model and QMoM." *Comptes Rendus Mecanique* 337.6 (2009): 449-457.

[14] Marchisio, Daniele L., and Rodney O. Fox. "Solution of population balance equations using the direct quadrature method of moments." *Journal of Aerosol Science* 36.1 (2005): 43-73.

[15] McGraw, Robert. "Description of aerosol dynamics by the quadrature method of moments." *Aerosol Science and Technology* 27.2 (1997): 255-265.

[16] McGraw, Robert, and Douglas L. Wright. "Chemically resolved aerosol dynamics for internal mixtures by the quadrature method of moments." *Journal of Aerosol Science* 34.2 (2003): 189-209.

[17] Serio, Michael A., et al. "Kinetics of volatile product evolution in coal pyrolysis: experiment and theory." Energy & Fuels 1.2 (1987): 138-152.

[18] Valipour, Mohammad Sadegh, and Yadollah Saboohi. "Modeling of multiple noncatalytic gas–solid reactions in a moving bed of porous pellets based on finite volume method." *Heat and Mass Transfer* 43.9 (2007): 881-894.

[19] Serban, Radu. sundialsTB v2.4.0, a matlab Interface to sundials. Technical Report UCRL-SM-212121, Lawrence Livermore National Laboratory, 2009.

[20] Cash, J. R. "Review paper: Efficient numerical methods for the solution of stiff initial-value problems and differential algebraic equations." *Proceedings of the Royal Society of London A: Mathematical, Physical and Engineering Sciences*. Vol. 459. No. 2032. The Royal Society, 2003.

[21] Singer, Simcha Lev. Gasification and combustion modeling for porous char particles. Diss. Massachusetts Institute of Technology, 2012.

[22] Singer, Simcha, Cai, Jianghuai, and Green, William H. "Detailed modeling of pyrolysis of large lignite particles." *Clearwater Coal Conference,*2015

[23] Yang, He, et al. "Simulation of the Evolution of Pressure in a Lignite Particle during Pyrolysis." *Energy & Fuels* 28.5 (2014): 3511-3518.

[24] Zhao, Yuxin, Michael A. Serio, and Peter R. Solomon. "A general model for devolatilization of large coal particles." *Symposium (International) on Combustion*. Vol. 26. No. 2. Elsevier, 1996.

[25] Patankar, Suhas. *Numerical heat transfer and fluid flow*. CRC press, 1980.

[26] Marchisio, Daniele L. *Quadrature method of moments for poly-disperse flows*. Springer Vienna, 2007.

[27] Zhang, Kai, Changfu You, and Yulei Li. "Experimental and numerical investigation on the pyrolysis of single coarse lignite particles." *Korean Journal of Chemical Engineering* 29.4 (2012): 540-548.

[28] Wang, Ying, et al. "Lignite temperature distribution during low temperature carbonization process in an industrial width carbonization furnace." *Fuel Processing Technology* 144 (2016): 85-94.

[29] Paprika, Milijana, et al. "Experimental and Numerical Investigation of the Primary Fragmentation of a Lignite during Fluidized-Bed (FB) Devolatilization." *Energy & Fuels* 29.5 (2015): 3394-3398.

[30] Genetti, Dominic, Thomas H. Fletcher, and Ronald J. Pugmire. "Development and application of a correlation of 13C NMR chemical structural analyses of coal based on elemental composition and volatile matter content." Energy & Fuels 13.1 (1999): 60-68.

[31] King, C. Judson. *Separation processes*. Courier Corporation, 2013.

[32] Lima, Eduardo RA, Marcelo Castier, and Evaristo C. Biscaia Jr. "Differential-algebraic approach to dynamic simulations of flash drums with rigorous evaluation of physical properties." *Oil & Gas Science and Technology-Revue de l'IFP* 63.5 (2008): 677-686.

Appendix

Table A-1. Kinetic Rate Coefficients of Various Light Gas Species (Taken from Bib. 10)

Gas	Primary functional group source	Gas fraction	A(s^{-1})	E/R (K)
CO_2 extra loose	carboxyl	0.022	0.56×10^{15}	30000±1500
CO_2 loose	carboxyl	0.022	0.65×10^{17}	33850±1500
CO_2 tight	carboxyl	0.030	0.11×10^{16}	38315±2000
H_2O loose	hydroxyl	0.045	0.22×10^{19}	30000±1500
H_2O tight	hydroxyl	0.00001	0.17×10^{14}	32700±1500
CO ether loose	ether O	0.060	0.14×10^{19}	40000±6000
CO ether tight	ether O	0.063	0.15×10^{16}	40500±1500
HCN loose		0.010	0.17×10^{14}	30000±1500
HCN tight		0.016	0.69×10^{13}	42500±4750
NH_3		0.00001	0.12×10^{13}	27300±3000
CH_x aliphatics	H(al)	0.081	0.84×10^{15}	30000±1500
CH_4 extra loose	methoxy	0.011	0.84×10^{15}	30000±1500
CH_4 loose	methyl	0.011	0.75×10^{14}	30000±2000
CH_4 tight	methyl	0.022	0.34×10^{12}	30000±2000
H aromatic	H(ar)	0.016	0.10×10^{15}	40500±6000
CO extra tight	ether O	0.00001	0.20×10^{14}	45500±1500
S organic		0.038	0.20×10^{14}	40000±5000